

<sup>1</sup> Multi-temporal drought and its effects on land cover change and vegetation  
<sup>2</sup> productivity in continental Chile

<sup>3</sup> Francisco Zambrano<sup>a,1,\*</sup>, Anton Vrieling<sup>b</sup>, Francisco Fernández<sup>c</sup>, Francisco Meza, Ionel Duran-Llacer,  
<sup>4</sup> Alejandro Venegas-González, Nicolas Raab, Dylan Craven

<sup>a</sup> Universidad Mayor, Hémera Centro de Observación de la Tierra, Facultad de Ciencias, Escuela de Ingeniería en Medio Ambiente y Sustentabilidad, Santiago, Chile, 7500994

<sup>b</sup> University of Twente, Faculty of Geo-Information Science and Earth Observation (ITC), Enschede, The Netherlands,

<sup>c</sup> Universidad San Sebastián,

---

<sup>5</sup> **Abstract**

The north-central region of Chile has been the focus of research studies due to the persistent decrease in water supply, which is impacting the hydrological system and vegetation development. This persistent period of water scarcity has been defined as a megadrought. The aim of our study is to evaluate the land cover change over continental Chile and to examine how this is connected to drought indices of water supply, atmospheric evaporative demand (AED), soil moisture, and their effects on vegetation productivity. The drought indices were derived using monthly ERA5-Land reanalysis data spanning from 1981 to 2023. The Moderate-Resolution Imaging Spectroradiometer (MODIS) datasets were utilized to obtain information on annual land cover and monthly vegetation productivity. We analyzed short- (1, 3, 6 months) to long-term (12, 24, 36 months) time scales of drought. Our results showed that land cover change was highest in the south-central part of the country, reaching changes as high as 36% in the surface type. The water demand has increased for the whole country, with a major increase in the north. The AED and soil moisture evidence a decreasing trend, which decreases at longer time scales and from north to south. The extreme south part of the country shows an increase in supply. Vegetation productivity has a negative trend in the north-central region for all land cover types. On the other hand, forests seem to be the most resistant type to drought. The types that show to be most affected by variation in climate conditions are shrublands, savannas, and croplands. The drought indices that have the capability of explaining to a major degree the variance in vegetation productivity are the ones that consider soil moisture for twelve months and the combined effect of precipitation and AED for 24 and 12 months. The results indicate that the north-central region is the most sensitive to water supply deficits lasting longer than a year.

<sup>6</sup> **Keywords:** drought, land cover change, satellite

---

<sup>7</sup> **1. Introduction**

<sup>8</sup> Drought is often classified as meteorological when there is a decrease in precipitation below the mean  
<sup>9</sup> average of several years (more than 30 years), hydrological when these anomalies last for long periods (months  
<sup>10</sup> to years) and affect water systems, and agricultural when the deficit impacts plant health anomalies and  
<sup>11</sup> leads to decreased productivity (Wilhite and Glantz, 1985). However, it is important to note that drought

---

\*Corresponding author

Email addresses: francisco.zambrano@umayor.cl (Francisco Zambrano), a.vrieling@utwente.nl (Anton Vrieling), francisco.fernandez@uss.cl (Francisco Fernández)

<sup>1</sup>This is the first author footnote.

is also influenced by human activities, which were not considered in the definitions. Thus, Van Loon et al. (2016) and AghaKouchak et al. (2021) have given an updated definition of drought for the Anthropocene, suggesting that it should be considered the feedback of humans' decisions and activities that drives the anthropogenic drought. Simultaneously, drought leads to heightened tree mortality and induces alterations in land cover and land use, ultimately affecting ecosystems (Crausbay et al., 2017). Even though many ecological studies have misinterpreted how to characterize drought, for example, sometimes considering "dry" conditions as "drought" (Slette et al., 2019). Then, Crausbay et al. (2017) proposed the ecological drought definition as "an episodic deficit in water availability that drives ecosystems beyond thresholds of vulnerability, impacts ecosystem services, and triggers feedback in natural and/or human systems." In light of current global warming, it is crucial to study the interaction between drought and ecosystems in order to understand their feedback and impact on water security. (Bakker, 2012)

Human-induced greenhouse gas emissions have increased the frequency and/or intensity of drought as a result of global warming, according to the sixth assessment report (AR6) of the Intergovernmental Panel on Climate Change (IPCC) (Calvin et al., 2023). The evidence supporting this claim has been strengthened since AR5 (IPCC, 2013). Recent studies, however, have produced contrasting findings, suggesting that drought has not exhibited a significant trend over the past forty years. (Vicente-Serrano et al., 2022; Kogan et al., 2020). Vicente-Serrano et al. (2022) analyzed the meteorological drought trend on a global scale, finding that only in a few regions has there been an increase in the severity of drought. Moreover, they attribute the increase in droughts over the past forty years solely to an increase in atmospheric evaporative demand (AED), which in turn enhances vegetation water demand, with important implications for agricultural and ecological droughts. Also, they state that "the increase in hydrological droughts has been primarily observed in regions with high water demand and land cover change". Similarly, Kogan et al. (2020) analyzed the drought trend using vegetation health methods, finding that for the globe, hemispheres, and main grain-producing countries, drought has not expanded or intensified for the last 38 years. Further, the Masson-Delmotte (2021) suggests that there is a high degree of confidence that rising temperatures will increase the extent, frequency, and severity of droughts. Also, AR6 (Calvin et al., 2023) predicts that many regions of the world will experience more severe agricultural and ecological droughts even if global warming stabilizes at 1.5°–2°C. To better evaluate the impact of drought trends on ecosystems, assessments are needed that relate meteorological and soil moisture variables to their effects on vegetation.

From 1960 to 2019, land use change has impacted around one-third of the Earth's surface, which is four times more than previously thought (Winkler et al., 2021). Multiple studies aim to analyze and forecast changes in land cover globally (Winkler et al., 2021; Song et al., 2018) and regionally (Chamling and Bera, 2020; Homer et al., 2020; Yang and Huang, 2021). Some others seek to analyze the impact of land cover change on climate conditions such as temperature and precipitation (Luyssaert et al., 2014; Pitman et al., 2012). There is less research on the interaction between drought and land cover change (Chen et al., 2022; Akinyemi, 2021; Peng et al., 2017). Peng et al. (2017) conducted a worldwide investigation utilizing net primary production to examine the spatial and temporal variations in vegetation productivity at global level. The study aimed to assess the influence of drought by comparing the twelve-month Standardized Precipitation Evapotranspiration Index (SPEI) and land cover change. According to their findings, drought is responsible for 37% of the decline in vegetation productivity, while water availability accounts for 55% of the variation. Chen et al. (2022) studied the trend of vegetation greenness and productivity and its relation to meteorological drought (SPEI of twelve months in December) and soil moisture at the global level. The results showed lower correlations (<0.2) for both variables. Akinyemi (2021) evaluates drought trends and land cover change using vegetation indices in Botswana in a semi-arid climate. These studies mostly looked at how changes in land cover and vegetation productivity are related to a single drought index (SPEI) over a single time period of 12 months. SPEI takes into account the combined effect of precipitation and AED as a water balance, but it does not allow us to know the contribution of each variable on its own. Some things worth investigating in terms of land cover change and vegetation productivity are: i) How do they respond to short- to long-term meteorological droughts? ii) How do they behave in humid and arid climatic zones regarding drought? And iii) What is the role of soil moisture? Likewise, there is a lack of understanding of how the alteration in water supply and demand is affecting land cover transformations.

Chile's diverse climatic and ecosystem types (Beck et al. (2023);Luebert and Pliscoff (2022)) make it an ideal natural laboratory for studying climate and ecosystems. Additionally, the country has experienced severe drought conditions that have had significant effects on vegetation and water storage. Central Chile faced a persistent precipitation deficit between 2010 and 2022, defined as a megadrought (Garreaud et al., 2017), which has impacted the Chilean ecosystem. This megadrought was defined by the Standardized Precipitation Index (SPI) of twelve months in December having values below one standard deviation. Some studies have addressed how this drought affects single ecosystems in terms of forest development (Miranda et al., 2020; Venegas-González et al., 2018), forest fire occurrence (Urrutia-Jalabert et al., 2018), and crop productivity (Zambrano, 2023; Zambrano et al., 2018, 2016). We found one study regarding land cover and drought in Chile. The study by Fuentes et al. (2021) evaluates water scarcity and land cover change in Chile between 29° and 39° of south latitude. Fuentes et al. (2021) used the SPEI of one month for evaluating drought, which led to misleading results. For example, they did not find a temporal trend in the SPEI but found a decreasing trend in water availability and an increase trend on AED, which in turn should have been capable of being captured with longer time scales of the SPEI. The term "megadrought" in Chile is used to describe a prolonged water shortage that lasts for several years, resulting in a permanent deficit that impacts the hydrological system (Boisier et al., 2018). Hence, it is imperative to assess temporal scales that take into account the cumulative effect within some years. There is little knowledge about the relationship between drought and ecosystem in Chile; thus, it is important to understand in more detail how meteorological and soil moisture droughts influence ecosystem dynamics to inform adaptation options.

A detailed spatiotemporal assessment of the interaction of drought for short- to long-term and land cover change requires information on vegetation as well as weather variables such as precipitation, temperature, and soil moisture. Weather networks in Chile present some disadvantages, such as spatio-temporal gaps, a short history, and irregular quality, which make them difficult to represent the whole extent of the country spatially. In order to do this, we use reanalysis data from ERA5-Land (Muñoz-Sabater et al., 2021) to create drought indices that consider AED, precipitation, and soil moisture over a range of time periods, from the short to the long term. Also, we use vegetation spectral information and annual land cover change from the Moderate-Resolution Imaging Spectroradiometer (MODIS). We expect to gain insight regarding the temporal evolution of water demand, water supply, and soil moisture, as well as the interaction with land cover change and vegetation productivity. Here, we analyze the multi-dimensional impacts of drought across ecosystems in continental Chile. More specifically, we aim to assess: i) temporal changes in land-use cover and the direction and magnitude of their relationships with drought indices for water demand and supply, soil moisture, and vegetation productivity; ii) short- to long-term temporal trends in multi-scalar drought indices; and iii) the relationship between vegetation productivity and drought indices for water demand and supply and soil moisture across Chilean ecosystems.

## 2. Study area

Continental Chile has a diverse climate conditions with strong gradients from north to south and east to west (Aceituno et al., 2021) (Figure 1 a), which determines its great ecosystem diversity (Luebert and Pliscoff (2022)) (Figure 1 c). The Andes Mountains are a main factor in climate latitudinal variation (Garreaud, 2009). In order to characterize the climate and ecosystem of Chile, we utilize the Köppen-Geiger classification system developed by Beck et al. (2023) and the land cover data derived from the MODIS product for the period of 2001–2022, based on the International Geosphere-Biosphere Programme (IGBP) classification scheme proposed by Friedl and Sulla-Menashe (2019). “Norte Grande” and “Norte Chico” predominate in an arid desert climate with hot (Bwh) and cold (Bwk) temperatures. At the south of “Norte Chico,” the climate changes to an arid steppe with cold temperatures (Bsk). In these two northern regions, the land is mostly bare, with a minor surface of vegetation types such as shrubland and grassland. In the zones “Centro” and the north half of “Sur,” the main climate is Mediterranean, with warm to hot summers (Csa and Csb). Land cover in “Centro” comprises a significant amount of shrubland and savanna (50%), grassland (16%), forest (8%), and croplands (5%). An oceanic climate (Cfb) predominates in the south of “Sur” and the north of “Austral.” Those zones are high in forest and grassland. The southern part of

112 the country has a tundra climate, and in “Austral”, it is a cold semi-arid area with an extended surface of  
 113 grassland, forest, and, to a lesser extent, savanna.

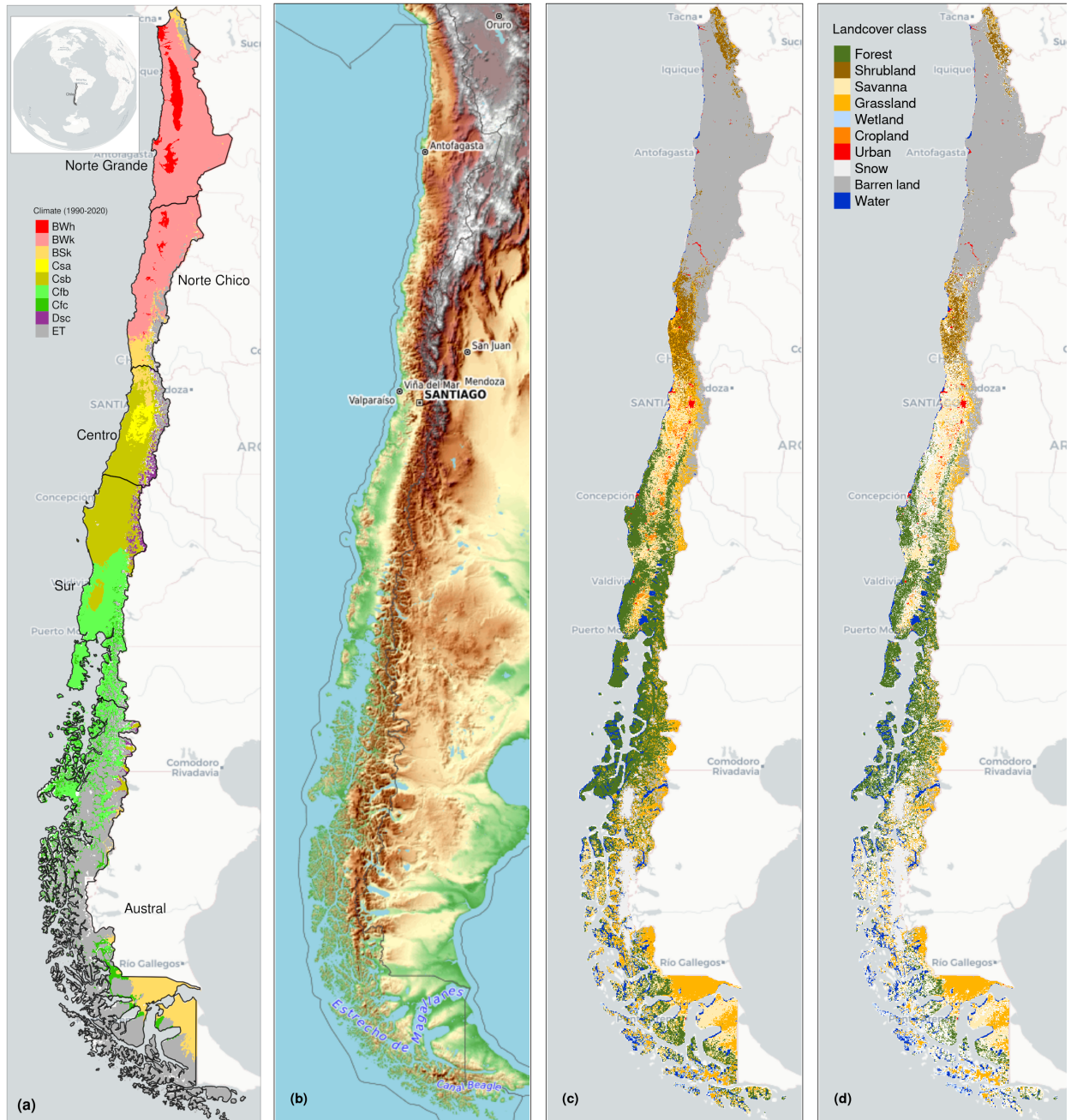


Figure 1: (a) Chile with the Koppen-Geiger climate classes and the five macrozones “Norte Grande”, “Norte Chico”, “Centro”, “Sur”, and “Austral”. (b) Topography reference map. (c) land cover classes for 2022. (d) Persistent land cover classes (> 80%) for 2001-2022

114 **3. Materials and Methods**

115 *3.1. Data*

116 *3.1.1. Gridded meteorological and vegetation data*

117 To analyze the LULCC, we use the IGBP scheme from the MCD12Q1 collection 6.1 from MODIS. This  
 118 product has a yearly frequency from 2001 to 2022. The IGBP defines 17 classes; from these, we regrouped  
 119 into ten macroclasses, as follows: classes 1-4 to forest, 5-7 to shrublands, 8-9 to savannas, 10 as grasslands,  
 120 11 as wetlands, 12 and 14 to croplands, 13 as urban, 15 as snow and ice, 16 as barren, and 17 to water  
 121 bodies. Thus, we have a land cover raster time series with the ten classes for 2001 and 2023. Prior to  
 122 using this class, we compared it with the types of land cover made by Zhao et al. (2016), which is a more  
 123 detailed land cover map of Chile with a 30 m spatial resolution for 2012–2013. It reached a global accuracy  
 124 of ~0.82. The procedure of validation is demonstrated in Section S1 of the supplementary material. To derive  
 125 a proxy for vegetation productivity, we used the MOD13A3 collection 6.1 product from MODIS (Didan,  
 126 2015). It provides vegetation indices (NDVI and EVI) at 1km of spatial resolution and monthly frequency.  
 127 The MOD13A3 and MCD12Q1 were retrieved from the online Data Pool, courtesy of the NASA EOSDIS  
 128 Land Processes Distributed Active Archive Center (LP DAAC), USGS Earth Resources Observation and  
 129 Science (EROS) Center, Sioux Falls, South Dakota, <https://lpdaac.usgs.gov/tools/data-pool/>.

Table 1: Description of the earth observation data used

Product	Sub-product	Variable	Spatial Resolution	Period	Units	Short Name
ERA5L		Precipitation	0.1°	1981-2023	mm	P
		Maximum temperature			°C	T <sub>max</sub>
		Minimum temperature			°C	T <sub>min</sub>
		Volumetric Soil Water Content at 1m			m3/m3	SM
ERA5L*	MOD13A3.061	Atmospheric Evaporative Demand	0.1°	1981-2023	mm	AED
MODIS		Normalized Difference Vegetation Index	1 km	2000-2023		NDVI
	MCD12Q1.061	land cover IGBP scheme		2001-2022		land cover

\*Derived from ERA5L with Eq. 1.

130 For soil moisture, water supply, and water demand variables, we used ERA5L (Muñoz-Sabater et al., 2021),  
 131 a reanalysis dataset that provides the evolution of the meteorological and soil moisture variables since 1950.  
 132 It has a spatial resolution of 0.1° (9 km), hourly frequency, and global coverage. We selected the variables  
 133 for total precipitation, maximum and minimum temperature at 2 meters, and volumetric soil water layers  
 134 between 0 and 100cm of depth (layer 1 to layer 3).

135 *3.2. Land cover change and trend*

136 To analyze the LULCC, we use the IGBP scheme from the MCD12Q1 collection 6.1 from MODIS. Zambrano  
 137 et al. (2018) and Fuentes et al. (2021) have previously used this product for studies of drought and land  
 138 cover. The MCD12Q1 has a yearly frequency from 2001 to 2022. The IGBP defines 17 classes; from these,  
 139 we regrouped into ten macroclasses, as follows: classes 1-4 to forest, 5-7 to shrublands, 8-9 to savannas, 10  
 140 as grasslands, 11 as wetlands, 12 and 14 to croplands, 13 as urban, 15 as snow and ice, 16 as barren, and 17  
 141 to water bodies. Thus, we have a land cover raster time series with the ten macroclasses for 2001 and 2023.  
 142 We validate the land cover macroclasses regarding a highly detailed (30 m of spatial resolution) land cover  
 143 map made for Chile by Zhao et al. (2016) for 2013-2014. Our results showed a global accuracy of ~0.82 and  
 144 a F1 score of ~0.66. Section S2 in the Supplementary Material shows the procedure for validation.

145 Climate, vegetation development, seasonality, and changes in vegetation type all have an impact on the  
 146 time series of NDVI. In this study, we want to examine the variation in vegetation productivity across various  
 147 land cover types and how water demand, water supply, and soil moisture affect it. In order to avoid changes

148 due to a change in the land cover type that will wrongly impact NDVI, we developed a persistence mask for  
149 land cover for 2001–2022. Thereby, we reduce an important source of variation on a regional scale. Therefore,  
150 we generated a raster mask for IGBP MODIS per pixel using macroclasses that remained unchanged for at  
151 least 80% of the years (2001–2022). This enabled us to identify regions where the land cover macroclasses  
152 are persistent. We calculated the surface occupied per land cover class into the five macrozones (“Norte  
153 Grande” to “Austral”) per year for 2001–2023. After that, we calculated the trend’s change in surface per  
154 type. We used the Sen’ slope ([Sen, 1968](#)) based on Mann-Kendall ([Kendall, 1975](#)).

155 *3.3. Trend of drought and interaction to land cover change*

156 *3.3.1. Atmospheric Evaporative Demand (AED)*

157 In order to compute the drought indices that uses water demand, it is necessary to first calculate the AED.  
158 To do this, we employed the Hargreaves technique ([Hargreaves, 1994](#); [Hargreaves and Samani, 1985](#)), by  
159 applying the following equation:

$$AED = 0.0023 \cdot Ra \cdot (T + 17.8) \cdot (T_{max} - T_{min})^{0.5} \quad (1)$$

160 where  $Ra$  ( $MJ\ m^2\ day^{-1}$ ) is extraterrestrial radiation;  $T$ ,  $T_{max}$ , and  $T_{min}$  are mean, maximum, and  
161 minimum temperature ( $^{\circ}C$ ). We calculate the centroid coordinates per pixel and use the latitude to estimate  
162  $Ra$ .

163 We chose the method of Hargreaves to estimate AED because of its simplicity, which only requires tem-  
164 peratures and extrarrestrial radiation. Also, it has been recommended over other methods (e.g., Penman-  
165 Monteith) when the access to climatic variables is limited ([Vicente-Serrano et al., 2014](#)).

166 *3.3.2. Non-parametric calculation of drought indices*

167 To derive the drought indices of water supply and demand, soil moisture, and vegetation we used the ERA5L  
168 dataset and the MODIS product, with a monthly frequency for 1981–2023 and 2000–2023, respectively.

169 The drought indices correspond to a historical anomaly with regard to a variable (e.g., meteorological,  
170 vegetation, or soil moisture). To account for the anomaly, the common practice is to derive it following  
171 a statistical parametric methodology in which it is assumed that the statistical distribution of the data is  
172 known ([Heim \(2002\)](#)). A wrong decision is usually the highest source of uncertainty ([Laimighofer and Laaha  
\(2022\)](#)). In the case of Chile, due to its high degree of climatic variability, it is complex to choose a proper  
173 distribution without previous research. Here, we follow a non-parametric methodology for the calculation  
174 of the drought indices, in a similar manner as the framework proposed by [Farahmand and AghaKouchak  
\(2015\)](#); [Hobbins et al. \(2016\)](#); [McEvoy et al. \(2016\)](#).

175 For the purpose of monitoring water supply drought, we used the well-known Standardized Precipitation  
176 Index (SPI), which the World Meteorological Organization (WMO) recommended. The SPI solely relies on  
177 precipitation data. Also, it has been used worldwide for the study of drought, including in Chile ([Garreaud  
et al. \(2017\)](#); [Zambrano et al. \(2017\)](#)). The primary cause of drought is precipitation anomalies, and  
178 temperature usually makes it worse ([Luo et al. 2017](#)). Nowadays, there is an increase in attention toward  
179 using water demand separately to monitor droughts. ([Vicente-Serrano et al. \(2020\)](#); [Noguera et al. \(2022\)](#)).  
180 Thus, to evaluate water demand, we chose the Evaporative Demand Drought Index (EDDI), developed  
181 by [Hobbins et al. \(016\)](#) and [McEvoy et al. \(2016\)](#), which is based on the AED. EDDI is currently used for  
182 monitoring drought in the United States (<https://psl.noaa.gov/eddi/>). In our case, we used only temperature  
183 for AED, a difference from the original formulation of EDDI, which also considered wind besides temperature.  
184 To consider the combined effect of water supply and demand, we selected the SPEI, which corresponds to  
185 a balance between precipitation and AED. [Vicente-Serrano et al. \(2010\)](#) proposed the SPEI, and it has  
186 improved the SPI by incorporating temperature for drought monitoring. For SPEI, an auxiliary variable D  
187 = P-AED is calculated. Soil moisture is the main driver of vegetation productivity, particularly in semi-arid  
188 regions ([Li et al. \(2022\)](#)). Hence, for soil water drought, we used the SSI (Standardized Soil Moisture Index)  
189

<sup>192</sup> (Hao and AghaKouchak 2013; A. AghaKouchak 2014) which is a multi-scale index similar to SPI, SPEI, and  
<sup>193</sup> EDDI. In our case, for the SSI, we used the average soil moisture from ERA5L at 1m depth. Finally, for  
<sup>194</sup> the proxy of productivity, we used the zcNDVI proposed by Zambrano et al. (2018) which will be derived  
<sup>195</sup> from the NDVI retrieved from MOD13A1.

<sup>196</sup> To derive the drought indices, first we must calculate the sum of the variables with regard to the time scale  
<sup>197</sup> ( $s$ ). In this case, for generalization purposes, we will use  $V$ , referring to variables  $P$ ,  $AED$ ,  $D$ ,  $NDVI$ , and  
<sup>198</sup>  $SM$  (Table 1). We cumulated each  $V$  over the time series of  $n$  values (months), and for the time scales  $s$ :

$$A_{si} = \sum_{i=n-s-i+2}^{n-i+1} V_i \quad \forall i \geq n - s + 1 \quad (2)$$

<sup>199</sup> The  $A_{si}$  corresponds to a moving window (convolution) that sums the variable for time scales  $s$  from the  
<sup>200</sup> last month, month by month, until the first month in which it could sum for  $s$  months. Once the variable  
<sup>201</sup> is cumulated over time for the scale  $s$ . Thus, the empirically derived probabilities are obtained through an  
<sup>202</sup> inverse normal approximation (Abramowitz and Stegun, 1968). Then, we used the empirical Tukey plotting  
<sup>203</sup> position (Wilks, 2011) over  $A_i$  to derive the  $P(A_i)$  probabilities across a period of interest:

$$P(A_i) = \frac{i - 0.33}{n + 0.33} \quad (3)$$

<sup>204</sup> The drought indices  $SPI$ ,  $SPEI$ ,  $EDDI$ ,  $SSI$ , and  $zcNDVI$  are obtained following the inverse normal  
<sup>205</sup> approximation:

$$DI(A_i) = W - \frac{C_0 + C_1 \cdot W + c_2 \cdot W^2}{1 + d_1 \cdot W + d_2 \cdot W^2 + d_3 \cdot W^3} \quad (4)$$

<sup>206</sup>  $DI$  is referring to the drought index calculated for the variable  $V$ . The values for the constants are:  
<sup>207</sup>  $C_0 = 2.515517$ ,  $C_1 = 0.802853$ ,  $C_2 = 0.010328$ ,  $d_1 = 1.432788$ ,  $d_2 = 0.189269$ , and  $d_3 = 0.001308$ . For  
<sup>208</sup>  $P(A) \leq 0.5$ ,  $W = \sqrt{-2 \cdot \ln(P(A_i))}$ , and for  $P(A_i) > 0.5$ , replace  $P(A_i)$  with  $1 - P(A_i)$  and reverse the sign  
<sup>209</sup> of  $DI(A_i)$ .

<sup>210</sup> The drought indices were calculated for time scales of 1, 3, 6, 12, 24, and 36 months at a monthly frequency  
<sup>211</sup> for 1981–2023 in order to be used for short- to long-term evaluation of drought. In the case of the proxy of  
<sup>212</sup> vegetation productivity (zcNDVI) it was calculated for a time scale of six months at monthly frequency for  
<sup>213</sup> 2000–2023. For zcNDVI, we test time scales of 1, 3, 6, and 12 months; we choose to use six months because  
<sup>214</sup> that shows a more robust representation of vegetation productivity due to the seasonality of vegetation in  
<sup>215</sup> Chile.

### <sup>216</sup> 3.3.3. Trend of drought indices

<sup>217</sup> To estimate if there are significant positive or negative trends for the drought indices, we used the non-  
<sup>218</sup> parametric test of Mann-Kendall (Kendall, 1975). To determine the magnitude of the trend, we used Sen's  
<sup>219</sup> slope (Sen, 1968). Some of the advantages of applying this methodology are that the Sen's slope is not  
<sup>220</sup> affected by outliers as regular regression does, and it is a non-parametric method that is not influenced by  
<sup>221</sup> the distribution of the data. We applied Mann-Kendall to see if the trend was significant and Sen's slope  
<sup>222</sup> to estimate the magnitude of the trend. We did this to the six time scales from 1981 to 2023 (monthly  
<sup>223</sup> frequency) and the indices SPI, EDDI, SPEI, and SSI. Thus, we have trends per index and time scale (24 in  
<sup>224</sup> total). Then, we extracted the trend aggregated by macrozone and per land cover persistent macroclasses.

225    3.3.4. *Intercation drought indices and land cover change*

226    We wanted to explore the relationship between the trend in land cover classes and the trend in the drought  
227    indices. Regarding the trends of land cover obtained (see Section 3.4.5), we divide each trend (km<sup>2</sup>) per  
228    land cover class and macrozone by the total surface. That way, we relativize the trend regarding the total  
229    land cover surface type per zone. To the trends of the drought indices over Chile, we applied the mask of  
230    persistent land cover macroclass and aggregated the trend for land cover class and macrozone. We then  
231    explore visually the relationship between the trend of drought indices for the short- to long-term and the  
232    trend of land cover.

233    3.4. *Drought impacts on vegetation productivity within land cover*

234    We analyzed the trend of vegetation productivity over the unchanged land cover macroclasses. This way,  
235    we tried to reduce the noise in the vegetation due to a change in land cover from year to year. To achieve  
236    this, we will use the persistent mask of land cover macroclasses, which are the types that remain more than  
237    80% of the time for 2001–2022. We used this to evaluate the trend in zcNDVI per land cover class and  
238    macrozone.

239    We examine the drought indices of water demand, water supply, soil moisture, and their connection with  
240    vegetation productivity to investigate two main questions: i) whether short-term or long-term time scales  
241    have a greater impact on vegetation across Chile and its specific regions; and ii) the spatial variation  
242    in the strength of the correlation between the variables and time scales. Then, we will summarize for  
243    each land cover class and macrozone. Thus, we will be able to advance in understanding how climate  
244    is affecting vegetation, considering the impact on the five macroclasses of vegetation: forest, cropland,  
245    grassland, savanna, and shrubland.

246    We conducted an analysis on the linear correlation between the indices SPI, SPEI, EDDI, and SSI over  
247    time periods of 1, 3, 6, 12, 24, and 36 months, and zcNDVI. The objective is to determine the impact of  
248    soil moisture and water demand and supply on vegetation productivity. We used a method similar to that  
249    used by Meroni et al. (2017) which compared the SPI with the cumulative FAPAR (Fraction of Absorbed  
250    Photosynthetically Active Radiation). A pixel-to-pixel linear correlation analysis was performed for each  
251    index within the persistent mask of land cover macroclasses. To begin, the Pearson coefficient of correlation  
252    is computed for each of the six time scales. A significant time scale is identified as the one that attains the  
253    highest correlation ( $p < 0.05$ ). Subsequently, the Pearson correlation coefficient corresponding to the time  
254    scales at which the value peaked was extracted. As a result, for each index, we generated two raster maps:  
255    1) containing the raster with values of the time scales that reached the maximum correlation, and 2) having  
256    the value of the correlation obtained.

257    3.5. *Software and packages used*

258    For the downloading, processing, and analysis of the spatio-temporal data, we used the open source software  
259    for statistical computing and graphics, R (R Core Team, 2023). For downloading ERA5L, we used the  
260    {ecmwfr} package (Hufkens et al., 2019). For processing raster data, we used {terra} (Hijmans, 2023) and  
261    {stars} (Pebesma and Bivand, 2023). For managing vectorial data, we used {sf} (Pebesma, 2018). For  
262    the calculation of AED, we used {SPEI} (Beguería and Vicente-Serrano, 2023). For mapping, we use {tmap}  
263    (Tennekes, 2018). For data analysis, the suite {tidyverse} (Wickham et al., 2019) was used.

264    4. Results

265    5. Land cover change and trend

266    For vegetation, we obtained and use hereafter five macroclasses of land cover from IGBP MODIS: forest,  
267    shrubland, savanna, grassland, and croplands. Figure 1c shows the spatial distribution of the macroclasses  
268    through Chile for the year 2022. Figure 1d shows the macroclasses of land cover persistance (80%) during  
269    2021–2022, respectively (Table 2). Within continental Chile, barren land is the land cover class with the

Table 2: Surface of the land cover class that persist during 2001-2022

macrozone	Surface [km <sup>2</sup> ]					
	Forest	Cropland	Grassland	Savanna	Shrubland	Barren land
Norte Grande		886		7,910		171,720
Norte Chico		90	4,283	589	16,321	84,274
Centro	3,739	1,904	7,584	19,705	844	12,484
Sur	72,995	1,151	7,198	15,906		2,175
Austral	60,351		54,297	19,007	249	7,218
Total	—	137,085	3,145	74,247	55,206	25,324
						277,870

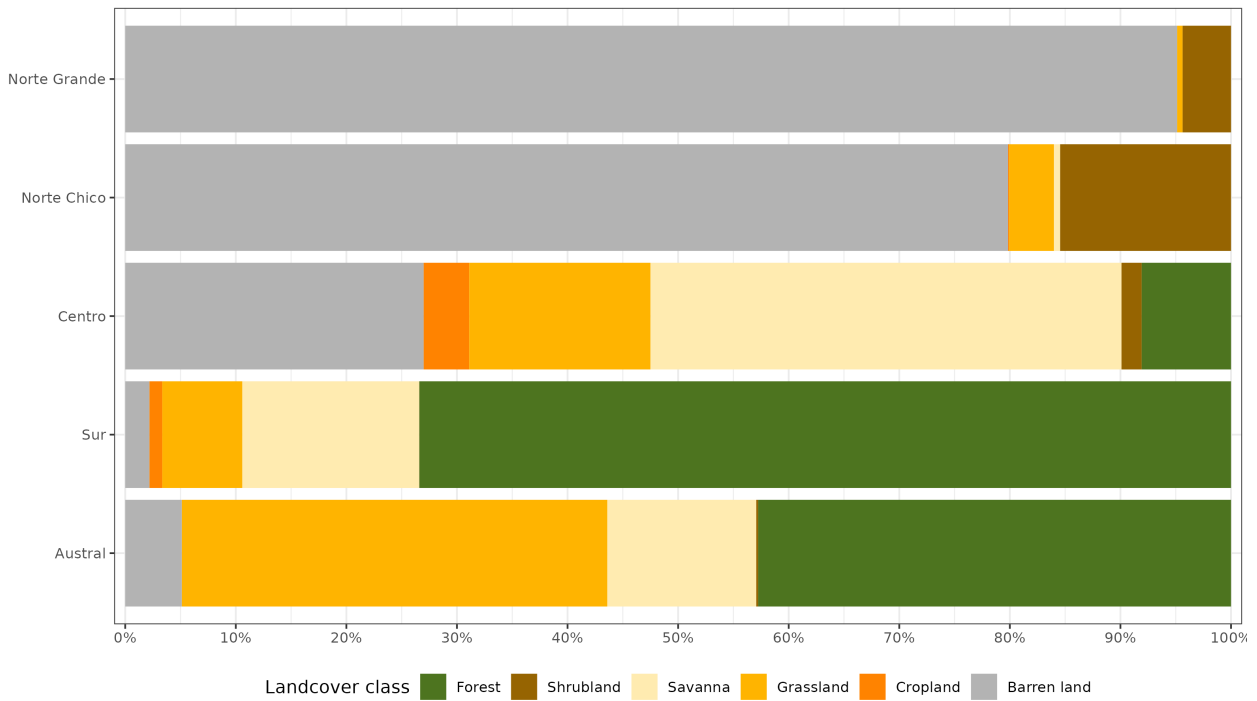


Figure 2: Proportion of land cover class from the persistent land cover for 2001-2022 (>80%) per macrozone

highest surface area (277,870 km<sup>2</sup>). The largest type of vegetation, with 137,085 km<sup>2</sup>, is forest. Grassland (74,247 km<sup>2</sup>), savanna (55,206 km<sup>2</sup>), shrubland (25,341 km<sup>2</sup>), and cropland (3,146 km<sup>2</sup>) are the other types (Table 2). The macrozones with major changes for 2001–2022 were “Centro,” “Sur,” and “Austral,” with 36%, 31%, and 34% of their surface changing the type of land cover, respectively (Figure 1 and Table 3). Figure 2 shows the summary of the proportion of surface per land cover class and macrozone, derived from the persistence mask over continental Chile.

The “Norte Chico” shows an increase in barren land of 111 km<sup>2</sup>yr<sup>-1</sup> and a reduction in the class savanna of 70 km<sup>2</sup>yr<sup>-1</sup>. In the “Centro” and “Sur,” there are changes with an important reduction in savanna (136 to 318 km<sup>2</sup>yr<sup>-1</sup>), and an increase in shrubland and grassland. Showing a change for more dense vegetation types. It appears to be a shift in the area cultivated (croplands) from the “Centro” to the “Sur.” Also, there is a high increase in forest (397 km<sup>2</sup>yr<sup>-1</sup> ) in the “Sur,” replacing the savanna lost (Table 3).

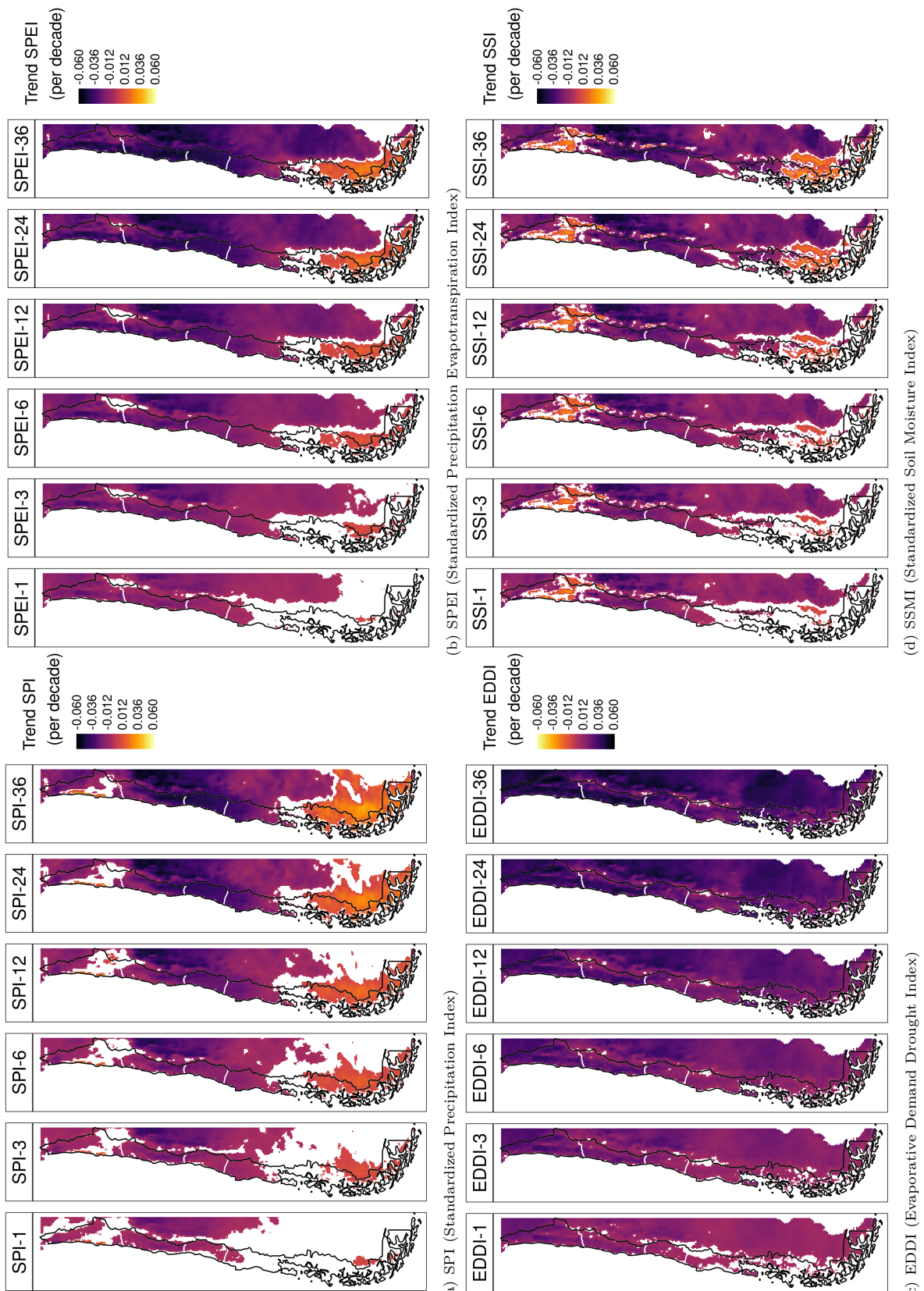
Table 3: The value of Sen's slope trend next to the time-series plot of surface per land cover class (IGBP MCD12Q1.016) for 2001–2022 through Central Chile. Values of zero indicate that there was not a significant trend. Red dots on the plots indicate the maximum and minimum values of surface.

macrozone	Trend of change [ $\text{km}^2 \text{ year}^{-1}$ ]											
	Forest		Cropland		Grassland		Savanna		Shrubland		Barren land	
	x	y	x	y	x	y	x	y	x	y	x	y
Norte Grande								0.0				0.0
Norte Chico					-12.1			0.0	-70.0		0.0	111.2
Centro		0.0			-22.4		83.2		-136.2		146.0	22.9
Sur		396.6			37.8		0.0		-318.8			0.0
Austral		0.0					0.0		172.1		-36.9	-93.2

281 5.1. Trend of drought and interaction to land cover change

282 5.1.1. Trend of drought indices

283 Figure 3 shows the spatial variation of the trend for the drought indices from short- to long-term scales.  
284 SPI and SPEI have a decreasing trend from “Norte Chico” to “Sur.” However, there is an increasing trend  
285 in “Austral.” The degree of the trend is stronger at higher time scales. The SSI indicates that in “Norte  
286 Grande,” there are surfaces that have increased in the southwest part and in the northeast have decreased,  
287 and is shown for all time scales. Similar to SPI and SPEI, SSI decreases at higher time scales. EDDI showed  
288 a positive trend for the whole of continental Chile, with a higher trend toward the north and a descending  
289 gradient toward the south. The degree of trend increases at higher time scales.



(c) EDDI (Evaporative Demand Drought Index)

Figure 3: Linear trend of the drought index (\*) at time scales of 1, 3, 6, 12, 24, and 36 months for 1981-2023

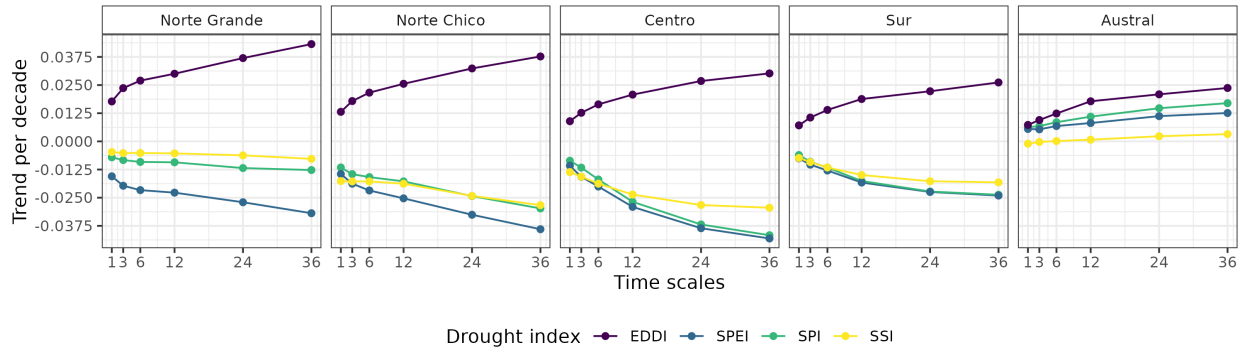


Figure 4: Trend per decade for the drought indices SPI, EDDI, SPEI, and SSI aggregated by macrozone.

In Figure 4, the averaged aggregation per macrozone, drought index, and time scale are shown. The macrozones that have the lowest trend are “Norte Chico” and “Centro,” where the SPI, SPEI, and SSI show that it decreases at longer time scales. Potentially explained due to the prolonged reduction in precipitation that has affected the hydrological system in Chile. At 36 months, it reaches trends between -0.03 and -0.04 (z-score) per decade for SPI, SPEI, and SSI. For “Sur,” the behavior is similar, decreasing at longer scales and having between -0.016 and -0.025 per decade for SPI, SPEI, and SSI. “Norte Grande” has the highest trend at 36 months for EDDI (0.042 per decade), and “Centro” has the lowest for SPI and SPEI. In “Norte Grande” and “Norte Chico,” which are in a semi-arid climate, it is evident that the EDDI has an effect on the difference between the SPI and SPEI index, which is not seen in the other macrozones. Contrary to the other macrozones, “Austral” showed an increase in all indices, being the highest for EDDI at 36 months (0.025) and the lowest for SSI, which shows only a minor increase in the trend.

### 5.1.2. Relationship between drought indices and land cover change

We look at the relationship between drought index and land cover change in Figure 5 by comparing the trends in land cover change (in terms of the total surface area per land cover type and macrozone) and drought indexes. Figure 5 shows that the negative trends in cropland (-0.029) and savanna (-0.026) in “Norte Chico” are the highest and are associated with an increase trend in EDDI and a decreasing trend in SPI, SPEI, and SSI. On the contrary, the shrubland in “Centro” has an increase (0.04) linked to a decrease in SPI, SPEI, and SSI and to an increase in EDDI. In “Austral,” the positive trend in shrubland fits with the positive trend in all the drought indices. The rest of the land cover types in the macrozones show weak associations with water supply, water demand, or soil moisture drought indices.

### 5.2. Drought impacts on vegetation productivity within land cover

#### 5.2.1. Vegetation productivity

In Figure 6 it is showed the spatial map of trends in zcNDVI ([fig-zcNDVI\_var]a) and the temporal variation of zcNDVI within the aggregated macrozones ([fig-zcNDVI\_var]b). In “Norte Grande,” vegetation productivity, as per the z-index, exhibits a yearly increase of 0.02 with respect to grassland and shrubland categories. There is a negative trend in “Norte Chico” with -0.04 and “Centro” with -0.02 per decade. In the “Norte Chico,” savanna (-0.05) has the lowest trend, and the rest of the types are around -0.04. In “Centro,” shrubland reaches -0.06, grassland -0.05, and croplands and savanna -0.01 per decade. This could be associated either with a reduction in vegetation surface, a decrease in biomass, or browning (Miranda et al., 2023). Vegetation reached its lowest values since the year 2019, with an extreme condition in early 2020 and 2022 in the “Norte Chico” and “Centro”. The “Sur” and “Austral” show a positive trend of around 0.016 per decade (Figure 6). Despite the croplands suffering from drought just as badly as the native vegetation in “Norte Chico,” the savanna and shrubland appears to be the region most affected by a negative trend in vegetation productivity.

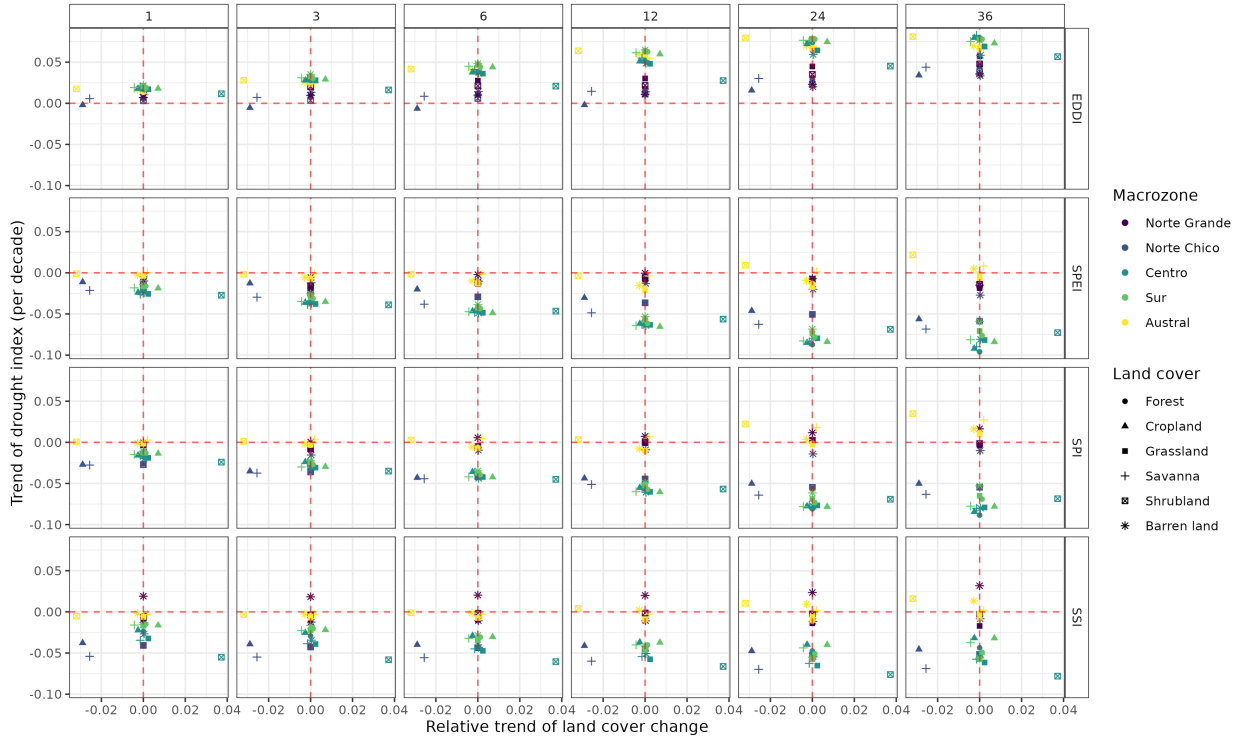


Figure 5: Relationship between the trend in land cover change and the trend in drought indices for the five macrozones. Vertical panels correspond to 1, 3, 6, 12, 24, and 36 months of the time scale by drought index. Horizontal panels show each drought index

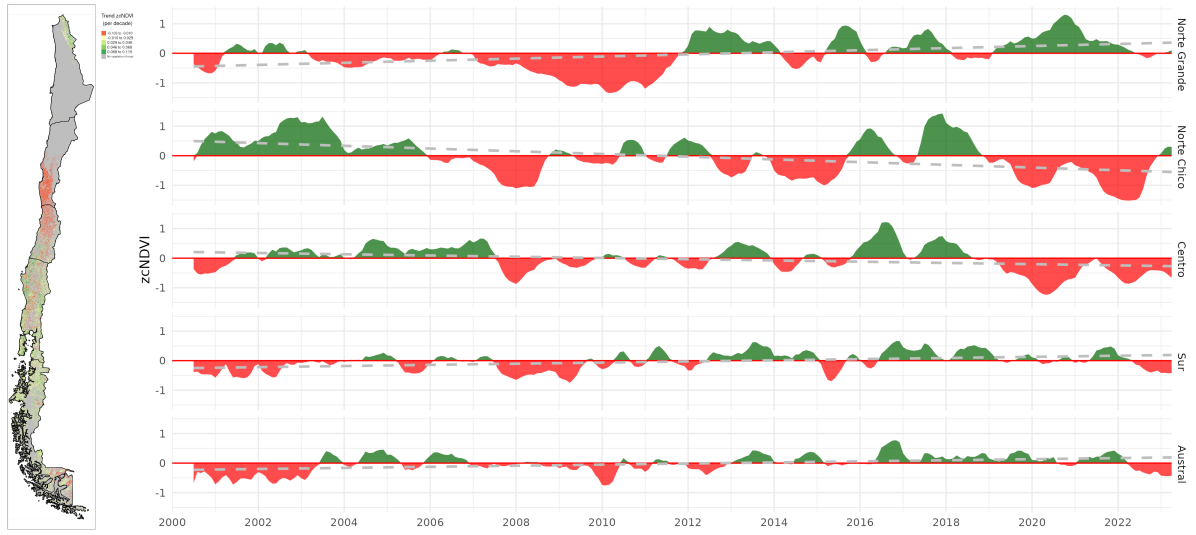


Figure 6: (a) Map of the linear trend of the index zcNDVI-6 for 2001–2023. Greener colors indicate a positive trend; redder colors correspond to a negative trend and a decrease in vegetation productivity. Grey colors indicate either no vegetation or a change in land cover type for 2001–2022. (b) Temporal variation of zcNDVI-6 aggregated at macrozone level within continental Chile. Each horizontal panel corresponds to a macrozone from ‘Norte Grande’ to ‘Austral’.

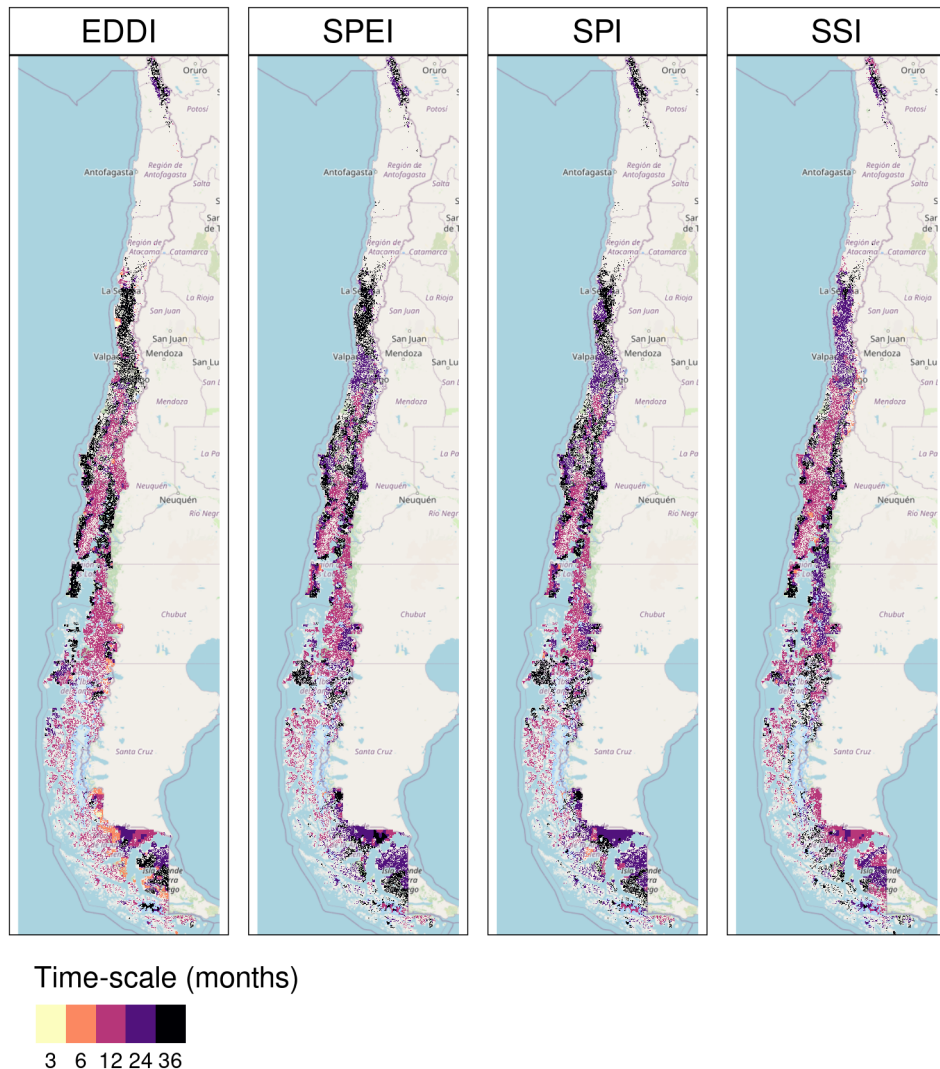


Figure 7: Time scales per drought index that reach the maximum coefficient of determination

### 5.2.2. Correlation between vegetation productivity and drought indices

Figure 7 is a map that shows the highest coefficient of determination ( $r^2$ , or  $rsq$ ) found in the regression analysis between different drought indicators and plant productivity over time. The spatial variation of time scales reached per index is mostly for time scales above 12 months. In the case of SSI, the predominant scales are 6 and 12 months. For all indices, to the north, the time scales are higher and diminish toward the south until the south part of “Austral” increases. In Figure 8, the map of Pearson correlation values is shown. The EDDI reached correlations above 0.5 between “Norte Chico” and “Sur.” The correlation changes from negative to positive toward the Andes Mountains and to the sea, just as in the northern part of “Austral.” The SPI and SPEI have similar results, with the higher values in “Norte Chico” and “Centro” being higher than 0.6. Following a similar spatial pattern as EDDI. The SSI showed to be the index that has a major spatial extension with a higher correlation. It has a similar correlation to SPI and SPEI for “Norte Chico” and “Sur,” but has improvements for “Sur.”

In Table 4, we aggregate per macrozone and landcover the correlation analysis presented in Figure 7 and Figure 8. According to what is shown, forests seem to be the most resistant to drought. Showing that

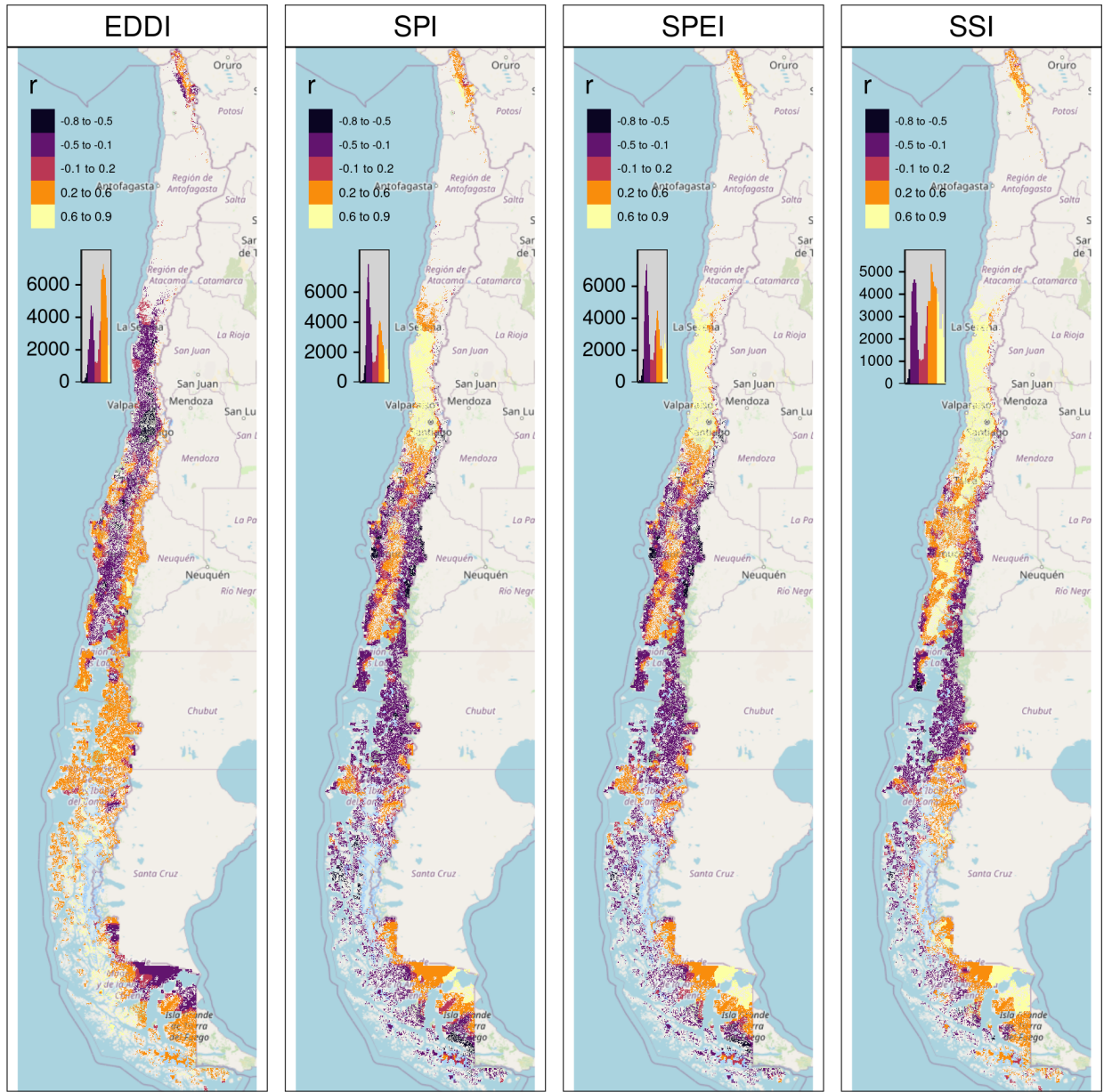


Figure 8: Pearson correlation value for the time scales and drought index that reach the maximum coefficient of determination

only “Centro” is slightly ( $rsq = 0.25$ ) impacted by a 12-month soil moisture deficit (SSI-12). In the “Norte Chico” and to a lesser extent in the “Norte Grande,” it is evident that a SSI-12 with a  $rsq = 0.45$  and a decrease in water supply (SPI-36 and SPEI-24 with  $rsq = 0.28$  and  $0.34$ , respectively) have an impact on grasslands. However, this type was unaffected by soil moisture, water supply, or demand in macrozones further south. The types that show to be most affected by variation in climate conditions are shrublands, savannas, and croplands. For savannas in “Norte Chico,” the SSI-12 and SPI-24 reached an  $rsq$  of  $0.74$  and  $0.58$ , respectively. This value decreases to the south, but the SSI-12 is still the variable explaining more of the variation in vegetation productivity ( $rsq = 0.45$  in “Centro” and  $0.2$  in “Sur”). In the case of croplands, the SPEI-12, SPI-36, and SSI-12 explain between  $45\%$  and  $66\%$  of the variability in “Norte

Table 4: Summary per land cover macroclass and macrozone regarding the correlation between zcNDVI with the drought indices EDDI, SPI, SPEI, and SSI for time scales of 1, 3, 6, 12, 24, and 36. The numbers in each cell indicate the time scale that reached the maximum correlation for the land cover and macrozone, and the color indicates the strength of the r-squared obtained with the index and the time scale.

	Forest				Cropland				Grassland				Savanna				Shrubland															
macrozone	EDDI	SPI	SPEI	SSI	EDDI	SPI	SPEI	SSI	EDDI	SPI	SPEI	SSI	EDDI	SPI	SPEI	SSI	EDDI	SPI	SPEI	SSI												
Norte Grande									36	36	36	12					36	12	36	12												
Norte Chico					36	36	12	12	36	36	24	12	36	24	24	12	36	36	24	12												
Centro	36	36	12	6	12	12	6	6	12	12	12	36	12	12	12	36	24	24	12													
Sur	36				6	6	6	6	6	6	6	12	6	6	6	6																
Austral	6	6									6	12	12	6	6	12																
 r-squared																																
347	Chico.” The type of land most impacted by climatic variation was shrubland, where soil moisture explained																															
348	59% and precipitation, 37%, in “Norte Chico” and “Centro,” with SSI-12 being the most relevant variable,																															
349	then SPI-36 in “Norte Chico” and SPI-24 in “Sur.”																															

## 350 6. Discussion

### 351 6.1. Drought trend and attribution to land cover

352 Vicente-Serrano et al. (2022), in a study at the global scale of drought trends, indicate that there have not  
 353 been significant trends in meteorological drought since 1950. Also, state that the increase in hidrological  
 354 trend in some parts of the globe (northeast Brazil and the Mediterranean region) is related to changes in land  
 355 cover and specifically to the rapidly increasing irrigated area, which consequently increases water extraction.  
 356 Kogan et al. (2020) analyzed the agricultural drought impact globally and in the main grain producer  
 357 countries, finding that “since 1980, the Earth warming has not changed the drought area or intensity.” In  
 358 our study, we considered the variation in vegetation productivity in Chile for areas without changes in land  
 359 cover, to avoid misleading conclusions that could be related to the increase in water demand due to land  
 360 cover change. Our results show a contrasting perspective. There has been a significant trend in the decline  
 361 of vegetation productivity (zcNDVI) since 2000 for “Norte Chico” and “Centro,” which has been extreme  
 362 between 2020 and 2022, seemsly due to an intense hydrological drought due to the persistance of the mega  
 363 drought (Garreaud et al., 2017). However, a rise in irrigated land doesn’t seem to have an impact on this  
 364 hydrological drought. Despite using the persistance mask for vegetation’s trend analysis, cropland, which  
 365 is the most water-demand type, showed a decrease trend in “Norte Chico” and “Centro.” Also, there was  
 366 an increase in barren land for both types. These changes are associated with a decrease in water demand  
 367 from vegetation. Nonetheless, we used the persistant land cover to ensure that the pixel has the same class;  
 368 in the case of croplands, it could happen that some areas had changed crops for others with higher water  
 369 consumption and consequently increase water demand. But this effect should be minor compared to the  
 370 results from land cover change at this scale of analysis.

371 On the other hand, for “Norte Chico” and “Centro,” our results show a decrease in trends of water supply  
 372 (SPI and SSI), which are higher at larger time scales, which is evidence of the hydrological drought. We say  
 373 that what happened in central Chile goes against what has been found on a global scale (Vicente-Serrano  
 374 et al., 2022; Kogan et al., 2020). This shows that the main cause of the hydrological drought in Chile was  
 375 a steady drop in water supply made worse by an increase in AED, but it seems that in zones most affected  
 376 by drought, the main cause is not an increase in water demand by vegetation like irrigated crops. Finally,

377 north-central Chile has experienced a decline in vegetation productivity across all macroclasses, which is  
378 primarily attributable to variations in water supply and soil moisture. An increase in water demand, such  
379 as an increase in the surface area of irrigated crops, could strengthen this trend.

380 *6.2. Land cover types and their impact by drought*

381 We discovered that croplands, savannas, and shrubland are the most susceptible to climatic changes and are  
382 most affected by the 12-month soil moisture deficit. In a study in the Yangtze River Basin in China, [Jiang et al. \(2020\)](#) analyzed the impact of drought on vegetation using the SPEI and the Enhanced Vegetation  
383 Index (EVI). They found that cropland was more sensitive to drought than grassland, showing that cropland  
384 responds strongly to short- and medium-term drought (< SPEI-6). In our case, the SPEI-12 was the one that  
385 most impacted the croplands in “Norte Chico” and “Centro.” In general, most studies show that croplands  
386 are most sensitive to short-term drought (< SPI-6) ([Zambrano et al., 2016](#); [Potopová et al., 2015](#); [Dai et al.,](#)  
387 [2020](#); [Rhee et al., 2010](#)). Short-term precipitation deficits impact soil water, and thus less water is available  
388 for plant growth. However, we found that in “Norte Chico,” an SPI-36 and SPEI-12 had a higher impact,  
389 which are associated with hydrological drought (long-term), and in “Centro,” an SPI-12 and SPEI-12. Thus,  
390 we attribute this impact to the hydrological drought that has decreased groundwater storage ([Taucare et al.,](#)  
391 [2024](#)), which in turn is impacted by long-term deficits, and consequently, the vegetation is more dependent on  
392 groundwater. In “Sur” and “Austral,” the correlations between drought indices and vegetation productivity  
393 decrease, as do the time scales that reach the maximum r-squared. What can be explained is that, south of  
394 “Centro,” predominate forest and grassland, the most resistant types. Also, drought episodes have been less  
395 frequent and intense. The drought episodes have had a lower impact on water availability for vegetation.  
396

397 According to [Senf et al. \(2020\)](#), severe drought conditions in Europe are a significant cause of tree mortality.  
398 However, we found that forest is the type of land cover macroclass less affected by variation in drought indices,  
399 being the most resistant land cover class to drought. Supporting this is [Fathi-Tapersht et al. \(2022\)](#), who  
400 assert that Indian forests are the most drought-resistant and recover rapidly. Similarly, the work of [Wu et al. \(2024\)](#), who analyzed vegetation loss and recovery in response to meteorological drought in the humid  
401 subtropical Pearl River basin in China, indicates that forests showed higher drought resistance. Using  
402 Vegetation Optical Depth (VOD), kNDVI, and EVI, [Xiao et al. \(2023\)](#) test the resistance of ecosystems  
403 and find that ecosystems with more forests are better able to handle severe droughts than croplands. They  
404 attribute the difference to a deeper rooting depth of trees, a higher water storage capacity, and different  
405 water use strategies between forest and cropland ([Xiao et al., 2023](#)).

406 In contrast to what we obtained, [Venegas-González et al. \(2023\)](#), who studied *Cryptocarya alba* and  
407 *Beilschmiedia miersii* (both from the Lauraceae family) that live in sclerophyllous forests in Chile, found  
408 that the trees’ overall growth had slowed down. This could mean that the natural dynamics of their forests  
409 have changed. They attributed it to the cumulative effects of the unprecedented drought (i.e., hydrological  
410 drought). Thus, we attribute that forest to being the most resistant to drought, due to the fact that most  
411 of the species comprising it are highly resilient to water scarcity compared to the other land cover classes.  
412 Nonetheless, if we want to go deep in our analysis, we should use earth observation data that is able to  
413 capture a higher level of detail. For example, when we used MOD13A3 with a 1km spatial resolution to  
414 measure vegetation condition, it took the average condition of 1 square kilometer. Then, to use remote  
415 sensing to look at how a certain type of forest (like sclerophyllous forest) changes in response to drought on  
416 a local level, we should use operational products with higher spatial resolutions, like those from Landsat or  
417 Sentinel. This will let us do a more thorough analysis.

418 *6.3. Soil moisture, vegetation productivity, and agricultural drought.*

419 The main external factors that affect biomass production by vegetation are actual evapotranspiration and  
420 soil moisture, and the rate of ET in turn depends on the availability of water storage in the root zone.  
421 Thus, soil moisture plays a key role in land carbon uptake and, consequently, in the production of biomass  
422 ([Humphrey et al., 2021](#)). Moreover, [Zhang et al. \(2022\)](#) indicate there is a bidirectional causality between  
423 soil moisture and vegetation productivity. Lastly, some studies have redefined agricultural drought as soil

moisture drought from a hydrological perspective (Van Loon et al., 2016; Samaniego et al., 2018). Even though soil moisture is the external factor most determinant of vegetation biomass, there are multiple internal factors, such as species, physiological characteristics, and plant hydraulics, that would affect vegetation productivity. Because of that, we believe that agricultural drought, referring to the drought that impacts vegetation productivity, is the most proper term, as originally defined by Wilhite and Glantz (1985).

The study results showed that the soil moisture-based drought index (SSI) was better at explaining vegetation productivity across land cover macroclasses than meteorological drought indices like SPI, SPEI, and EDDI. In the early growing season and especially in irrigated rather than rainfed croplands, soil moisture has better skills than SPI and SPEI for estimating gross primary production (GPP). This according to Chatterjee et al. (2022) evaluation of the SPI and SPEI and their correlation with GPP in the CONUS. Also, Zhou et al. (2021) indicate that the monthly scaled Standardized Water Deficit Index (SWDI) can accurately show the effects of agricultural drought in most of China. Nicolai-Shaw et al. (2017) also looked at the time-lag between the SWDI and the Vegetation Condition Index (VCI). They found that there was little to no time-lag in croplands but a greater time-lag in forests.

In our case, there is strong spatial variability throughout Chile and between classes, mainly attributable to climate heterogeneity, hydrological status, or vegetation resistance to water scarcity. The semi-arid “Norte Chico” and the Mediterranean “Centro” were where SSI had the best performance. In Chile, medium-term deficits of 12 months are more relevant in the response of vegetation, which decreases to the south, and in the case of croplands, they seem to react in a shorter time, with six months (SSI-6) in “Centro.” This variation for croplands could be related to the fact that in “Norte Chico,” the majority of crops are irrigated, but to the south there is a higher proportion of rainfed agriculture, which is most dependent on the short-term availability of water. Rather, in the “Norte Chico,” the orchards are more dependent on the storage of water in dams of groundwater reservoirs, which are affected by long-term drought (e.g., SPI-36).

#### 6.4. Future outlook (to complete)

### 7. Conclusion

There is a trend toward decreasing water supply in most parts of Chile, particularly in the “Centro” and “Norte Chico” regions. The whole country showed an increase in AED. Vegetation productivity only showed a decrease in the “Norte Chico” and “Centro,” being highest for shrubland and croplands. Forest is the land cover most resistant to drought, as shown along Chile, and shrubland and cropland are the most sensitive.

A soil moisture deficit of 12 months (SSI-12) is highly correlated with vegetation productivity for the land cover classes of shrubland, savannas, croplands, and forest in “Norte Chico” and “Centro.” For the southern part of the country with humid conditions, the correlation with SSI decreases. Soil moisture overcomes the capacity to explain vegetation productivity over the supply and demand drought indices in the entire territory.

The variation in vegetation productivity appears to be associated with climate variation rather than anthropogenic factors (e.g., an increase in water demand by irrigated crops). Even though switching to more demanding crops on the land could increase the impact of drought on vegetation, this would need to be more thoroughly investigated, for instance at the watershed level.

The results of this study could help in the development of a robust forecasting system for land cover classes in Chile, helping to improve preparedness for climate change impacts on vegetation.

### Supplementary material

### References

- Abramowitz, M., Stegun, I.A., 1968. Handbook of mathematical functions with formulas, graphs, and mathematical tables. volume 55. US Government printing office.

- 469 Aceituno, P., Boisier, J.P., Garreaud, R., Rondanelli, R., Rutllant, J.A., 2021. Climate and Weather in Chile, in: Fernández,  
 470 B., Gironás, J. (Eds.), Water Resources of Chile. Springer International Publishing, Cham. volume 8, pp. 7–29. URL:  
 471 [http://link.springer.com/10.1007/978-3-030-56901-3\\_2](http://link.springer.com/10.1007/978-3-030-56901-3_2).
- 472 AghaKouchak, A., Mirchi, A., Madani, K., Di Baldassarre, G., Nazemi, A., Alborzi, A., Anjileli, H., Azarderakhsh, M., Chiang,  
 473 F., Hassanzadeh, E., Huning, L.S., Mallakpour, I., Martinez, A., Mazdiyasni, O., Moftakhari, H., Norouzi, H., Sadegh,  
 474 M., Sadeqi, D., Van Loon, A.F., Wanders, N., 2021. Anthropogenic Drought: Definition, Challenges, and Opportunities. *Reviews of Geophysics* 59, e2019RG000683. URL: <https://agupubs.onlinelibrary.wiley.com/doi/10.1029/2019RG000683>, doi:[10.1029/2019RG000683](https://doi.org/10.1029/2019RG000683).
- 475 Akinyemi, F.O., 2021. Vegetation Trends, Drought Severity and Land Use-Land Cover Change during the Growing Season in  
 476 Semi-Arid Contexts. *Remote Sensing* 2021, Vol. 13, Page 836 13, 836. URL: <https://www.mdpi.com/2072-4292/13/5/836>  
 477 htm, doi:[10.3390/RS13050836](https://doi.org/10.3390/RS13050836). publisher: Multidisciplinary Digital Publishing Institute.
- 478 Bakker, K., 2012. Water Security: Research Challenges and Opportunities. *Science* 337, 914–915. URL: <https://www.science.org/doi/10.1126/science.1226337>, doi:[10.1126/science.1226337](https://doi.org/10.1126/science.1226337).
- 479 Beck, H.E., McVicar, T.R., Vergopolan, N., Berg, A., Lutsko, N.J., Dufour, A., Zeng, Z., Jiang, X., van Dijk, A.I.J.M., Miralles,  
 480 D.G., 2023. High-resolution (1 km) Köppen-Geiger maps for 1901–2099 based on constrained CMIP6 projections. *Scientific  
 481 Data* 10. URL: <http://dx.doi.org/10.1038/s41597-023-02549-6>, doi:[10.1038/s41597-023-02549-6](https://doi.org/10.1038/s41597-023-02549-6).
- 482 Beguería, S., Vicente-Serrano, S.M., 2023. SPEI: Calculation of the Standardized Precipitation-Evapotranspiration Index. URL:  
 483 <https://CRAN.R-project.org/package=SPEI>.
- 484 Boisier, J.P., Alvarez-Garreton, C., Cordero, R.R., Damiani, A., Gallardo, L., Garreaud, R.D., Lambert, F., Ramallo, C.,  
 485 Rojas, M., Rondanelli, R., 2018. Anthropogenic drying in central-southern Chile evidenced by long-term observations  
 486 and climate model simulations. *Elementa* 6, 74. URL: <https://www.elementascience.org/article/10.1525/elementa.328/>,  
 487 doi:[10.1525/elementa.328](https://doi.org/10.1525/elementa.328).
- 488 Calvin, K., Dasgupta, D., Krinner, G., Mukherji, A., Thorne, P.W., Trisos, C., Romero, J., Aldunce, P., Barrett, K., Blanco,  
 489 G., Cheung, W.W., Connors, S., Denton, F., Diongue-Niang, A., Dodman, D., Garschagen, M., Geden, O., Hayward, B.,  
 490 Jones, C., Jotzo, F., Krug, T., Lasco, R., Lee, Y.Y., Masson-Delmotte, V., Meinshausen, M., Mintenbeck, K., Moksit, A.,  
 491 Otto, F.E., Pathak, M., Pirani, A., Poloczanska, E., Pörtner, H.O., Revi, A., Roberts, D.C., Roy, J., Ruane, A.C., Skea,  
 492 J., Shukla, P.R., Slade, R., Slangen, A., Sokona, Y., Sörensson, A.A., Tignor, M., Van Vuuren, D., Wei, Y.M., Winkler,  
 493 H., Zhai, P., Zommers, Z., Hourcade, J.C., Johnson, F.X., Pachauri, S., Simpson, N.P., Singh, C., Thomas, A., Totin, E.,  
 494 Arias, P., Bustamante, M., Elgizouli, I., Flato, G., Howden, M., Méndez-Vallejo, C., Pereira, J.J., Pichs-Madruga, R., Rose,  
 495 S.K., Saheb, Y., Sánchez Rodríguez, R., Ürge Vorsatz, D., Xiao, C., Yassa, N., Alegría, A., Armour, K., Bednar-Friedl, B.,  
 496 Blok, K., Cissé, G., Dentener, F., Eriksen, S., Fischer, E., Garner, G., Guiavarch, C., Haasnoot, M., Hansen, G., Hauser, M.,  
 497 Hawkins, E., Hermans, T., Kopp, R., Leprince-Ringuet, N., Lewis, J., Ley, D., Ludden, C., Niamir, L., Nicholls, Z., Some,  
 498 S., Szopa, S., Trewin, B., Van Der Wijst, K.I., Winter, G., Witting, M., Birt, A., Ha, M., Romero, J., Kim, J., Haites, E.F.,  
 499 Jung, Y., Stavins, R., Birt, A., Ha, M., Orendain, D.J.A., Ignon, L., Park, S., Park, Y., Reisinger, A., Cammaramo, D.,  
 500 Fischlin, A., Fuglestvedt, J.S., Hansen, G., Ludden, C., Masson-Delmotte, V., Matthews, J.R., Mintenbeck, K., Pirani, A.,  
 501 Poloczanska, E., Leprince-Ringuet, N., Péan, C., 2023. IPCC, 2023: Climate Change 2023: Synthesis Report. Contribution  
 502 of Working Groups I, II and III to the Sixth Assessment Report of the Intergovernmental Panel on Climate Change [Core  
 503 Writing Team, H. Lee and J. Romero (eds.)]. IPCC, Geneva, Switzerland. Technical Report. Intergovernmental Panel on  
 504 Climate Change (IPCC). URL: <https://www.ipcc.ch/report/ar6/syr/>.
- 505 Chamling, M., Bera, B., 2020. Spatio-temporal Patterns of Land Use/Land Cover Change in the Bhutan–Bengal Foothill Region  
 506 Between 1987 and 2019: Study Towards Geospatial Applications and Policy Making. *Earth Systems and Environment* 4,  
 507 117–130. URL: <http://link.springer.com/10.1007/s41748-020-00150-0>, doi:[10.1007/s41748-020-00150-0](https://doi.org/10.1007/s41748-020-00150-0).
- 508 Chatterjee, S., Desai, A.R., Zhu, J., Townsend, P.A., Huang, J., 2022. Soil moisture as an essential component for delineating  
 509 and forecasting agricultural rather than meteorological drought. *Remote Sensing of Environment* 269, 112833. URL: <https://linkinghub.elsevier.com/retrieve/pii/S0034425721005538>, doi:[10.1016/j.rse.2021.112833](https://doi.org/10.1016/j.rse.2021.112833).
- 510 Chen, J., Shao, Z., Huang, X., Zhuang, Q., Dang, C., Cai, B., Zheng, X., Ding, Q., 2022. Assessing the impact of drought-  
 511 land cover change on global vegetation greenness and productivity. *Science of The Total Environment* 852, 158499. URL:  
 512 <https://linkinghub.elsevier.com/retrieve/pii/S004896972205598X>, doi:[10.1016/j.scitotenv.2022.158499](https://doi.org/10.1016/j.scitotenv.2022.158499).
- 513 Crausbay, S.D., Ramirez, A.R., Carter, S.L., Cross, M.S., Hall, K.R., Bathke, D.J., Betancourt, J.L., Colt, S., Cravens, A.E.,  
 514 Dalton, M.S., Dunham, J.B., Hay, L.E., Hayes, M.J., McEvoy, J., McNutt, C.A., Moritz, M.A., Nislow, K.H., Raheem, N.,  
 515 Sanford, T., 2017. Defining Ecological Drought for the Twenty-First Century. *Bulletin of the American Meteorological Society*  
 516 98, 2543–2550. URL: <https://journals.ametsoc.org/view/journals/bams/98/12/bams-d-16-0292.1.xml>, doi:[10.1175/BAMS-D-16-0292.1](https://doi.org/10.1175/BAMS-D-16-0292.1). publisher: American Meteorological Society.
- 517 Dai, M., Huang, S., Huang, Q., Leng, G., Guo, Y., Wang, L., Fang, W., Li, P., Zheng, X., 2020. Assessing agricultural drought  
 518 risk and its dynamic evolution characteristics. *Agricultural Water Management* 231, 106003. URL: <https://linkinghub.elsevier.com/retrieve/pii/S0378377419316531>, doi:[10.1016/j.agwat.2020.106003](https://doi.org/10.1016/j.agwat.2020.106003).
- 519 Didan, K., 2015. MOD13Q1 MODIS/Terra Vegetation Indices 16-Day L3 Global 250m SIN Grid V006. Technical Report.  
 520 NASA EOSDIS Land Processes DAAC. doi:[http://dx.doi.org/10.5067/MODIS/MOD13Q1.006](https://dx.doi.org/10.5067/MODIS/MOD13Q1.006).
- 521 Farahmand, A., AghaKouchak, A., 2015. A generalized framework for deriving nonparametric standardized drought indicators.  
 522 *Advances in Water Resources* 76, 140–145. URL: <https://linkinghub.elsevier.com/retrieve/pii/S0309170814002322>, doi:[10.1016/j.advwatres.2014.11.012](https://doi.org/10.1016/j.advwatres.2014.11.012).
- 523 Fathi-Taperasht, A., Shafizadeh-Moghadam, H., Minaei, M., Xu, T., 2022. Influence of drought duration and severity on  
 524 drought recovery period for different land cover types: evaluation using MODIS-based indices. *Ecological Indicators* 141,  
 525 109146. URL: <https://linkinghub.elsevier.com/retrieve/pii/S1470160X22006185>, doi:[10.1016/j.ecolind.2022.109146](https://doi.org/10.1016/j.ecolind.2022.109146).
- 526 Friedl, M., Sulla-Menashe, D., 2019. MCD12Q1 MODIS/Terra+Aqua Land Cover Type Yearly L3 Global 500m SIN Grid V006

- 534 [Data set]. NASA EOSDIS Land Processes DAAC. doi:[10.5067/MODIS/MCD12Q1.006](https://doi.org/10.5067/MODIS/MCD12Q1.006).
- 535 Fuentes, I., Fuster, R., Avilés, D., Vervoort, W., 2021. Water scarcity in central Chile: the effect of climate and land cover  
536 changes on hydrologic resources. *Hydrological Sciences Journal* 66, 1028–1044. URL: <https://www.tandfonline.com/doi/full/10.1080/02626667.2021.1903475>, doi:[10.1080/02626667.2021.1903475](https://doi.org/10.1080/02626667.2021.1903475).
- 537 Garreaud, R., Alvarez-Garreton, C., Barichivich, J., Boisier, J.P., Christie, D., Galleguillos, M., LeQuenne, C., McPhee, J.,  
538 Zambrano-Bigiarini, M., 2017. The 2010–2015 mega drought in Central Chile: Impacts on regional hydroclimate and  
539 vegetation. *Hydrology and Earth System Sciences Discussions* 2017, 1–37. URL: <http://www.hydrol-earth-syst-sci-discuss.net/hess-2017-191/>, doi:[10.5194/hess-2017-191](https://doi.org/10.5194/hess-2017-191).
- 540 Garreaud, R.D., 2009. The Andes climate and weather. *Advances in Geosciences* 22, 3–11. URL: <https://adgeo.copernicus.org/articles/22/3/2009/>, doi:[10.5194/adgeo-22-3-2009](https://doi.org/10.5194/adgeo-22-3-2009).
- 541 Hargreaves, G.H., 1994. Defining and Using Reference Evapotranspiration. *Journal of Irrigation and Drainage Engineering* 120,  
542 1132–1139. URL: <https://ascelibrary.org/doi/10.1061/%28ASCE%290733-9437%281994%29120%3A6%281132%29>, doi:[10.1061/\(ASCE\)0733-9437\(1994\)120:6\(1132\)](https://doi.org/10.1061/(ASCE)0733-9437(1994)120:6(1132)).
- 543 Hargreaves, G.H., Samani, Z.A., 1985. Reference crop evapotranspiration from temperature. *Applied engineering in agriculture*  
544 1, 96–99.
- 545 Heim, R.R., 2002. A Review of Twentieth-Century Drought Indices Used in the United States. *Bulletin of the American  
546 Meteorological Society* 83, 1149–1166. URL: <https://journals.ametsoc.org/doi/10.1175/1520-0477-83.8.1149>, doi:[10.1175/1520-0477-83.8.1149](https://doi.org/10.1175/1520-0477-83.8.1149).
- 547 Hijmans, R.J., 2023. terra: Spatial Data Analysis. URL: <https://CRAN.R-project.org/package=terra>.
- 548 Hobbins, M.T., Wood, A., McEvoy, D.J., Huntington, J.L., Morton, C., Anderson, M., Hain, C., 2016. The Evaporative Demand  
549 Drought Index. Part I: Linking Drought Evolution to Variations in Evaporative Demand. *Journal of Hydrometeorology* 17,  
550 1745–1761. URL: <http://journals.ametsoc.org/doi/10.1175/JHM-D-15-0121.1>, doi:[10.1175/JHM-D-15-0121.1](https://doi.org/10.1175/JHM-D-15-0121.1).
- 551 Homer, C., Dewitz, J., Jin, S., Xian, G., Costello, C., Danielson, P., Gass, L., Funk, M., Wickham, J., Stehman, S., Auch, R.,  
552 Riitters, K., 2020. Conterminous United States land cover change patterns 2001–2016 from the 2016 National Land Cover  
553 Database. *ISPRS Journal of Photogrammetry and Remote Sensing* 162, 184–199. URL: <https://linkinghub.elsevier.com/retrieve/pii/S0924271620300587>, doi:[10.1016/j.isprsjprs.2020.02.019](https://doi.org/10.1016/j.isprsjprs.2020.02.019).
- 554 Hufkens, K., Stauffer, R., Campitelli, E., 2019. The ecwmfr package: an interface to ECMWF API endpoints. URL: <https://bluegreen-labs.github.io/ecmwfr/>.
- 555 Humphrey, V., Berg, A., Ciais, P., Gentine, P., Jung, M., Reichstein, M., Seneviratne, S.I., Frankenberger, C., 2021. Soil  
556 moisture–atmosphere feedback dominates land carbon uptake variability. *Nature* 592, 65–69. URL: <https://www.nature.com/articles/s41586-021-03325-5>, doi:[10.1038/s41586-021-03325-5](https://doi.org/10.1038/s41586-021-03325-5).
- 557 IPCC, 2013. Climate Change 2013: The Physical Science Basis. Contribution of Working Group I to the Fifth Assessment  
558 Report of the Intergovernmental Panel on Climate Change. Cambridge University Press, Cambridge, UK; New York, USA.  
559 URL: [www.climatechange2013.org](http://www.climatechange2013.org), doi:[10.1017/CBO9781107415324](https://doi.org/10.1017/CBO9781107415324).
- 560 Jiang, W., Wang, L., Feng, L., Zhang, M., Yao, R., 2020. Drought characteristics and its impact on changes in surface  
561 vegetation from 1981 to 2015 in the Yangtze River Basin, China. *International Journal of Climatology* 40, 3380–3397. URL:  
562 <https://rnets.onlinelibrary.wiley.com/doi/10.1002/joc.6403>, doi:[10.1002/joc.6403](https://doi.org/10.1002/joc.6403).
- 563 Kendall, M., 1975. Rank correlation methods (4th ed. 2d impression). Griffin.
- 564 Kogan, F., Guo, W., Yang, W., 2020. Near 40-year drought trend during 1981–2019 earth warming and food security. *Geomatics,  
565 Natural Hazards and Risk* 11, 469–490. URL: <https://www.tandfonline.com/doi/full/10.1080/19475705.2020.1730452>, doi:[10.1080/19475705.2020.1730452](https://doi.org/10.1080/19475705.2020.1730452).
- 566 Laimighofer, J., Laaha, G., 2022. How standard are standardized drought indices? Uncertainty components for the SPI  
567 & SPEI case. *Journal of Hydrology* 613, 128385. URL: <https://linkinghub.elsevier.com/retrieve/pii/S0022169422009544>,  
568 doi:[10.1016/j.jhydrol.2022.128385](https://doi.org/10.1016/j.jhydrol.2022.128385).
- 569 Li, W., Migliavacca, M., Forkel, M., Denissen, J.M.C., Reichstein, M., Yang, H., Duveiller, G., Weber, U., Orth, R., 2022.  
570 Widespread increasing vegetation sensitivity to soil moisture. *Nature Communications* 13, 3959. URL: <https://www.nature.com/articles/s41467-022-31667-9>, doi:[10.1038/s41467-022-31667-9](https://doi.org/10.1038/s41467-022-31667-9).
- 571 Luebert, F., Pliscott, P., 2022. The vegetation of Chile and the EcoVeg approach in the context of the International Vegetation  
572 Classification project. *Vegetation Classification and Survey* 3, 15–28. URL: <https://vcs.pensoft.net/article/67893/>, doi:[10.3897/VCS.67893](https://doi.org/10.3897/VCS.67893).
- 573 Luyssaert, S., Jammet, M., Stoy, P.C., Estel, S., Pongratz, J., Ceschia, E., Churkina, G., Don, A., Erb, K., Ferlicq, M.,  
574 Gielen, B., Grünwald, T., Houghton, R.A., Klumpp, K., Knohl, A., Kolb, T., Kuemmerle, T., Laurila, T., Lohila, A.,  
575 Loustau, D., McGrath, M.J., Meyfroidt, P., Moors, E.J., Naudts, K., Novick, K., Otto, J., Pilegaard, K., Pio, C.A., Rambal,  
576 S., Rebmann, C., Ryder, J., Suyker, A.E., Varlagin, A., Wattenbach, M., Dolman, A.J., 2014. Land management and  
577 land-cover change have impacts of similar magnitude on surface temperature. *Nature Climate Change* 4, 389–393. URL:  
578 <https://www.nature.com/articles/nclimate2196>, doi:[10.1038/nclimate2196](https://doi.org/10.1038/nclimate2196).
- 579 Masson-Delmotte, V., P.Z.A.P.S.L.C.C.P.S.B.N.C.Y.C.L.G.M.I.G.M.H.K.L.E.L.J.B.R.M.T.K.M.T.W.O.Y.R.Y.a.B.Z.e., 2021.  
580 IPCC, 2021: Climate Change 2021: The Physical Science Basis. Contribution of Working Group I to the Sixth Assessment  
581 Report of the Intergovernmental Panel on Climate Change. Technical Report. URL: <https://www.ipcc.ch/>. publication  
582 Title: Cambridge University Press. In Press.
- 583 McEvoy, D.J., Huntington, J.L., Hobbins, M.T., Wood, A., Morton, C., Anderson, M., Hain, C., 2016. The Evaporative Demand  
584 Drought Index. Part II: CONUS-Wide Assessment against Common Drought Indicators. *Journal of Hydrometeorology* 17,  
585 1763–1779. URL: <http://journals.ametsoc.org/doi/10.1175/JHM-D-15-0122.1>, doi:[10.1175/JHM-D-15-0122.1](https://doi.org/10.1175/JHM-D-15-0122.1).
- 586 Meroni, M., Rembold, F., Fasbender, D., Vrieling, A., 2017. Evaluation of the Standardized Precipitation Index as an early  
587 predictor of seasonal vegetation production anomalies in the Sahel. *Remote Sensing Letters* 8, 301–310. URL: [20](http://www.</a></p>
</div>
<div data-bbox=)

- 599 [tandfonline.com/doi/abs/10.1080/2150704X.2016.1264020](https://tandfonline.com/doi/abs/10.1080/2150704X.2016.1264020), doi:[10.1080/2150704X.2016.1264020](https://doi.org/10.1080/2150704X.2016.1264020).
- 600 Miranda, A., Lara, A., Altamirano, A., Di Bella, C., González, M.E., Julio Camarero, J., 2020. Forest browning trends in  
601 response to drought in a highly threatened mediterranean landscape of South America. Ecological Indicators 115, 106401.  
602 URL: <https://linkinghub.elsevier.com/retrieve/pii/S1470160X20303381>, doi:[10.1016/j.ecolind.2020.106401](https://doi.org/10.1016/j.ecolind.2020.106401).
- 603 Miranda, A., Syphard, A.D., Berdugo, M., Carrasco, J., Gómez-González, S., Ovalle, J.F., Delpiano, C.A., Vargas, S.,  
604 Squeo, F.A., Miranda, M.D., Dobbs, C., Mentler, R., Lara, A., Garreaud, R., 2023. Widespread synchronous decline  
605 of Mediterranean-type forest driven by accelerated aridity. Nature Plants 9, 1810–1817. URL: <https://www.nature.com/articles/s41477-023-01541-7>, doi:[10.1038/s41477-023-01541-7](https://doi.org/10.1038/s41477-023-01541-7).
- 606 Muñoz-Sabater, J., Dutra, E., Agustí-Panareda, A., Albergel, C., Arduini, G., Balsamo, G., Boussetta, S., Choulga, M.,  
607 Harrigan, S., Hersbach, H., Martens, B., Miralles, D.G., Piles, M., Rodríguez-Fernández, N.J., Zsoter, E., Buontempo, C.,  
608 Thépaut, J.N., 2021. ERA5-Land: a state-of-the-art global reanalysis dataset for land applications. Earth System Science  
609 Data 13, 4349–4383. URL: <https://essd.copernicus.org/articles/13/4349/2021/>, doi:[10.5194/essd-13-4349-2021](https://doi.org/10.5194/essd-13-4349-2021).
- 610 Nicolai-Shaw, N., Zscheischler, J., Hirsch, M., Gudmundsson, L., Seneviratne, S.I., 2017. A drought event composite analysis  
611 using satellite remote-sensing based soil moisture. Remote Sensing of Environment 203, 216–225. URL: <https://linkinghub.elsevier.com/retrieve/pii/S0034425717302729>, doi:[10.1016/j.rse.2017.06.014](https://doi.org/10.1016/j.rse.2017.06.014).
- 612 Noguera, I., Vicente-Serrano, S.M., Domínguez-Castro, F., 2022. The Rise of Atmospheric Evaporative Demand Is Increasing  
613 Flash Droughts in Spain During the Warm Season. Geophysical Research Letters 49, e2021GL097703. URL: <https://agupubs.onlinelibrary.wiley.com/doi/10.1029/2021GL097703>, doi:[10.1029/2021GL097703](https://doi.org/10.1029/2021GL097703).
- 614 Pebesma, E., 2018. Simple Features for R: Standardized Support for Spatial Vector Data. The R Journal 10, 439–446. URL:  
615 <https://doi.org/10.32614/RJ-2018-009>, doi:[10.32614/RJ-2018-009](https://doi.org/10.32614/RJ-2018-009).
- 616 Pebesma, E., Bivand, R., 2023. Spatial Data Science: With applications in R. Chapman and Hall/CRC, London. URL:  
617 <https://r-spatial.org/book/>.
- 618 Peng, D., Zhang, B., Wu, C., Huete, A.R., Gonsamo, A., Lei, L., Ponce-Campos, G.E., Liu, X., Wu, Y., 2017. Country-level  
619 net primary production distribution and response to drought and land cover change. Science of The Total Environment 574,  
620 65–77. URL: <https://linkinghub.elsevier.com/retrieve/pii/S0048969716319507>, doi:[10.1016/j.scitotenv.2016.09.033](https://doi.org/10.1016/j.scitotenv.2016.09.033).
- 621 Pitman, A.J., De Noblet-Ducoudré, N., Avila, F.B., Alexander, L.V., Boisier, J.P., Brovkin, V., Delire, C., Cruz, F., Donat,  
622 M.G., Gayler, V., Van Den Hurk, B., Reick, C., Volodire, A., 2012. Effects of land cover change on temperature and  
623 rainfall extremes in multi-model ensemble simulations. Earth System Dynamics 3, 213–231. URL: <https://esd.copernicus.org/articles/3/213/2012/>, doi:[10.5194/esd-3-213-2012](https://doi.org/10.5194/esd-3-213-2012).
- 624 Potopová, V., Stepánek, P., Mozný, M., Türkott, L., Soukup, J., 2015. Performance of the standarised precipitation evapotranspiration index at various lags for agricultural drought risk assessment in the {C}zech {R}epublic. Agricultural and Forest Meteorology 202, 26–38.
- 625 R Core Team, 2023. R: A Language and Environment for Statistical Computing. R Foundation for Statistical Computing,  
626 Vienna, Austria. URL: <https://www.R-project.org/>.
- 627 Rhee, J., Im, J., Carbone, G.J., 2010. Monitoring agricultural drought for arid and humid regions using multi-sensor remote  
628 sensing data. Remote Sensing of Environment 114, 2875–2887. URL: <http://www.sciencedirect.com/science/article/pii/S003442571000221X>, doi:[10.1016/j.rse.2010.07.005](https://doi.org/10.1016/j.rse.2010.07.005).
- 629 Samaniego, L., Thober, S., Kumar, R., Wanders, N., Rakovec, O., Pan, M., Zink, M., Sheffield, J., Wood, E.F., Marx, A.,  
630 2018. Anthropogenic warming exacerbates European soil moisture droughts. Nature Climate Change 8, 421–426. URL:  
631 <https://www.nature.com/articles/s41558-018-0138-5>, doi:[10.1038/s41558-018-0138-5](https://doi.org/10.1038/s41558-018-0138-5).
- 632 Sen, P.K., 1968. Estimates of the Regression Coefficient Based on Kendall's Tau. Journal of the American Statistical Association  
633 63, 1379–1389. URL: <http://www.tandfonline.com/doi/abs/10.1080/01621459.1968.10480934>, doi:[10.1080/01621459.1968.10480934](https://doi.org/10.1080/01621459.1968.10480934).
- 634 Senf, C., Buras, A., Zang, C.S., Rammig, A., Seidl, R., 2020. Excess forest mortality is consistently linked to drought  
635 across Europe. Nature Communications 11, 6200. URL: <https://www.nature.com/articles/s41467-020-19924-1>, doi:[10.1038/s41467-020-19924-1](https://doi.org/10.1038/s41467-020-19924-1).
- 636 Slette, I.J., Post, A.K., Awad, M., Even, T., Punzalan, A., Williams, S., Smith, M.D., Knapp, A.K., 2019. How ecologists  
637 define drought, and why we should do better. Global Change Biology 25, 3193–3200. URL: <https://onlinelibrary.wiley.com/doi/10.1111/gcb.14747>, doi:[10.1111/gcb.14747](https://doi.org/10.1111/gcb.14747).
- 638 Song, X.P., Hansen, M.C., Stehman, S.V., Potapov, P.V., Tyukavina, A., Vermote, E.F., Townshend, J.R., 2018. Global land  
639 change from 1982 to 2016. Nature 560, 639–643. URL: <https://www.nature.com/articles/s41586-018-0411-9>, doi:[10.1038/s41586-018-0411-9](https://doi.org/10.1038/s41586-018-0411-9).
- 640 Taucare, M., Viguier, B., Figueiroa, R., Daniele, L., 2024. The alarming state of Central Chile's groundwater resources: A  
641 paradigmatic case of a lasting overexploitation. Science of The Total Environment 906, 167723. URL: <https://linkinghub.elsevier.com/retrieve/pii/S0048969723063507>, doi:[10.1016/j.scitotenv.2023.167723](https://doi.org/10.1016/j.scitotenv.2023.167723).
- 642 Tennekes, M., 2018. tmap: Thematic Maps in R. Journal of Statistical Software 84, 1–39. doi:[10.18637/jss.v084.i06](https://doi.org/10.18637/jss.v084.i06).
- 643 Urrutia-Jalabert, R., González, M.E., González-Reyes, , Lara, A., Garreaud, R., 2018. Climate variability and forest fires in  
644 central and south-central Chile. Ecosphere 9, e02171. URL: <https://esajournals.onlinelibrary.wiley.com/doi/10.1002/ecs2.2171>, doi:[10.1002/ecs2.2171](https://doi.org/10.1002/ecs2.2171).
- 645 Van Loon, A.F., Gleeson, T., Clark, J., Van Dijk, A.I., Stahl, K., Hannaford, J., Di Baldassarre, G., Teuling, A.J., Tallaksen,  
646 L.M., Uijlenhoet, R., Hannah, D.M., Sheffield, J., Svoboda, M., Verbeiren, B., Wagener, T., Rangecroft, S., Wanders, N.,  
647 Van Lanen, H.A., 2016. Drought in the Anthropocene. Nature Geoscience 9, 89–91. doi:[10.1038/ngeo2646](https://doi.org/10.1038/ngeo2646).
- 648 Venegas-González, A., Juñent, F.R., Gutiérrez, A.G., Filho, M.T., 2018. Recent radial growth decline in response to increased  
649 drought conditions in the northernmost Nothofagus populations from South America. Forest Ecology and Management 409,  
650 94–104. URL: <https://linkinghub.elsevier.com/retrieve/pii/S0378112717313993>, doi:[10.1016/j.foreco.2017.11.006](https://doi.org/10.1016/j.foreco.2017.11.006).

- 664 Venegas-González, A., Muñoz, A.A., Carpintero-Gibson, S., González-Reyes, A., Schneider, I., Gipolou-Zuñiga, T., Aguilera-Betti, I., Roig, F.A., 2023. Sclerophyllous Forest Tree Growth Under the Influence of a Historic Megadrought in the Mediterranean Ecoregion of Chile. *Ecosystems* 26, 344–361. URL: <https://link.springer.com/10.1007/s10021-022-00760-x>, doi:[10.1007/s10021-022-00760-x](https://doi.org/10.1007/s10021-022-00760-x).
- 665 Vicente-Serrano, S.M., Azorin-Molina, C., Sanchez-Lorenzo, A., Revuelto, J., López-Moreno, J.I., González-Hidalgo, J.C., Moran-Tejeda, E., Espejo, F., 2014. Reference evapotranspiration variability and trends in Spain, 1961–2011. *Global and Planetary Change* 121, 26–40. URL: <https://linkinghub.elsevier.com/retrieve/pii/S0921818114001180>, doi:[10.1016/j.gloplacha.2014.06.005](https://doi.org/10.1016/j.gloplacha.2014.06.005).
- 666 Vicente-Serrano, S.M., Beguería, S., López-Moreno, J.I., 2010. A multiscalar drought index sensitive to global warming: The standardized precipitation evapotranspiration index. *Journal of Climate* 23, 1696–1718. URL: <http://dx.doi.org/10.1175/2009JCLI2909.1>, doi:[10.1175/2009JCLI2909.1](https://doi.org/10.1175/2009JCLI2909.1).
- 667 Vicente-Serrano, S.M., Peña-Angulo, D., Beguería, S., Domínguez-Castro, F., Tomás-Burguera, M., Noguera, I., Gimeno-Sotelo, L., El Kenawy, A., 2022. Global drought trends and future projections. *Philosophical Transactions of the Royal Society A: Mathematical, Physical and Engineering Sciences* 380, 20210285. URL: <https://royalsocietypublishing.org/doi/10.1098/rsta.2021.0285>, doi:[10.1098/rsta.2021.0285](https://doi.org/10.1098/rsta.2021.0285).
- 668 Vicente-Serrano, S.M., McVicar, T.R., Miralles, D.G., Yang, Y., Tomas-Burguera, M., 2020. Unraveling the influence of atmospheric evaporative demand on drought and its response to climate change. *WIREs Climate Change* 11, e632. URL: <https://wires.onlinelibrary.wiley.com/doi/10.1002/wcc.632>, doi:[10.1002/wcc.632](https://doi.org/10.1002/wcc.632).
- 669 Wickham, H., Averick, M., Bryan, J., Chang, W., McGowan, L.D., François, R., Grolemund, G., Hayes, A., Henry, L., Hester, J., Kuhn, M., Pedersen, T.L., Miller, E., Bache, S.M., Müller, K., Ooms, J., Robinson, D., Seidel, D.P., Spinu, V., Takahashi, K., Vaughan, D., Wilke, C., Woo, K., Yutani, H., 2019. Welcome to the tidyverse. *Journal of Open Source Software* 4, 1686. doi:[10.21105/joss.01686](https://doi.org/10.21105/joss.01686).
- 670 Wilhite, D.A., Glantz, M.H., 1985. Understanding: The drought phenomenon: The role of definitions. *Water International* 10, 111–120. URL: <http://dx.doi.org/10.1080/02508068508686328>, doi:[10.1080/02508068508686328](https://doi.org/10.1080/02508068508686328).
- 671 Wilks, D.S., 2011. Empirical distributions and exploratory data analysis. *Statistical Methods in the Atmospheric Sciences* 100.
- 672 Winkler, K., Fuchs, R., Rounsevell, M., Herold, M., 2021. Global land use changes are four times greater than previously estimated. *Nature Communications* 12, 2501. URL: <https://www.nature.com/articles/s41467-021-22702-2>, doi:[10.1038/s41467-021-22702-2](https://doi.org/10.1038/s41467-021-22702-2).
- 673 Wu, C., Zhong, L., Yeh, P.J.F., Gong, Z., Lv, W., Chen, B., Zhou, J., Li, J., Wang, S., 2024. An evaluation framework for quantifying vegetation loss and recovery in response to meteorological drought based on SPEI and NDVI. *Science of The Total Environment* 906, 167632. URL: <https://linkinghub.elsevier.com/retrieve/pii/S0048969723062599>, doi:[10.1016/j.scitotenv.2023.167632](https://doi.org/10.1016/j.scitotenv.2023.167632).
- 674 Xiao, C., Zaehle, S., Yang, H., Wigneron, J.P., Schmullius, C., Bastos, A., 2023. Land cover and management effects on ecosystem resistance to drought stress. *Earth System Dynamics* 14, 1211–1237. URL: <https://esd.copernicus.org/articles/14/1211/2023/>, doi:[10.5194/esd-14-1211-2023](https://doi.org/10.5194/esd-14-1211-2023).
- 675 Yang, J., Huang, X., 2021. The 30 m annual land cover dataset and its dynamics in China from 1990 to 2019. *Earth System Science Data* 13, 3907–3925. URL: <https://essd.copernicus.org/articles/13/3907/2021/>, doi:[10.5194/essd-13-3907-2021](https://doi.org/10.5194/essd-13-3907-2021).
- 676 Zambrano, F., 2023. Four decades of satellite data for agricultural drought monitoring throughout the growing season in Central Chile, in: Vijay P. Singh Deepak Jhajharia, R.M., Kumar, R. (Eds.), *Integrated Drought Management*, Two Volume Set. CRC Press, p. 28.
- 677 Zambrano, F., Lillo-Saavedra, M., Verbist, K., Lagos, O., 2016. Sixteen years of agricultural drought assessment of the biobío region in chile using a 250 m resolution vegetation condition index (VCI). *Remote Sensing* 8, 1–20. URL: <http://www.mdpi.com/2072-4292/8/6/530>, doi:[10.3390/rs8060530](https://doi.org/10.3390/rs8060530). publisher: Multidisciplinary Digital Publishing Institute.
- 678 Zambrano, F., Vrieling, A., Nelson, A., Meroni, M., Tadesse, T., 2018. Prediction of drought-induced reduction of agricultural productivity in Chile from MODIS, rainfall estimates, and climate oscillation indices. *Remote Sensing of Environment* 219, 15–30. URL: <https://www.sciencedirect.com/science/article/pii/S0034425718304541>, doi:[10.1016/j.rse.2018.10.006](https://doi.org/10.1016/j.rse.2018.10.006). publisher: Elsevier.
- 679 Zambrano, F., Wardlow, B., Tadesse, T., Lillo-Saavedra, M., Lagos, O., 2017. Evaluating satellite-derived long-term historical precipitation datasets for drought monitoring in Chile. *Atmospheric Research* 186, 26–42. URL: <https://www.sciencedirect.com/science/article/pii/S0169809516305865>, doi:[10.1016/j.atmosres.2016.11.006](https://doi.org/10.1016/j.atmosres.2016.11.006). publisher: Elsevier.
- 680 Zhang, W., Wei, F., Horion, S., Fensholt, R., Forkel, M., Brandt, M., 2022. Global quantification of the bidirectional dependency between soil moisture and vegetation productivity. *Agricultural and Forest Meteorology* 313, 108735. URL: <https://linkinghub.elsevier.com/retrieve/pii/S0168192321004214>, doi:[10.1016/j.agrformet.2021.108735](https://doi.org/10.1016/j.agrformet.2021.108735).
- 681 Zhao, Y., Feng, D., Yu, L., Wang, X., Chen, Y., Bai, Y., Hernández, H.J., Galleguillos, M., Estades, C., Biging, G.S., Radke, J.D., Gong, P., 2016. Detailed dynamic land cover mapping of Chile: Accuracy improvement by integrating multi-temporal data. *Remote Sensing of Environment* 183, 170–185. URL: <https://linkinghub.elsevier.com/retrieve/pii/S0034425716302188>, doi:[10.1016/j.rse.2016.05.016](https://doi.org/10.1016/j.rse.2016.05.016).
- 682 Zhou, K., Li, J., Zhang, T., Kang, A., 2021. The use of combined soil moisture data to characterize agricultural drought conditions and the relationship among different drought types in China. *Agricultural Water Management* 243, 106479. URL: <https://linkinghub.elsevier.com/retrieve/pii/S0378377420305965>, doi:[10.1016/j.agwat.2020.106479](https://doi.org/10.1016/j.agwat.2020.106479).